The accumulation and dispersion of heavy particles in forced two-dimensional mixing layers. Part 2: The effect of gravity

N. Raju and E. Meiburg
Department of Aerospace Engineering, University of Southern California, Los Angeles, California 90089-1191

(Received 18 November 1994; accepted 21 February 1995)

The dispersion and settling of small, heavy, spherical particles in a temporally evolving two-dimensional mixing layer under gravity is investigated. The dilute limit is assumed, in which both the effect of the particles on the fluid flow and the interaction among the particles is negligible. The particle dynamics is quantified as a function of the dimensionless Stokes and Froude numbers, St and Fr, which express the ratios of the three time scales related to (i) the fluid flow, (ii) the particles' inertia, and (iii) their settling velocity, respectively. For horizontal flow in which the upper stream is the seeded one, the mixing layer accelerates the settling of particles with small St, whereas particles with large St are slowed down in their settling motion. At intermediate St and for moderate settling velocities, root-mean-square (RMS) data for the particle concentration field demonstrate the generation of strong inhomogeneities by the mixing layer. These regions of high particle concentration have the form of bands in the initially unseeded stream. Scaling laws for their angles and the distance between them are given. Furthermore, analytical results for linearized flow fields are derived that demonstrate the optimal efficiency of the dispersion and settling process at intermediate St. The numerical simulations show the existence of different parameter regimes, in which the particle motion is dominated by the coherent vortices and by gravity, respectively. Scaling laws are derived for the particle dispersion and settling for both of these regimes, which show reasonable quantitative agreement with the simulation data. Flows that exhibit a vortex pairing process show a reduced tendency of the particles toward suspension. For vertically upward flow in which the faster stream is seeded, is observed a sharp maximum in the particle dispersion measures for intermediate St and settling velocities equal to one-half the difference between the free-stream velocities. Under these conditions, the cross-stream fluid velocity components become optimally efficient in ejecting particles into the unseeded stream.

I. INTRODUCTION

The present study continues our computational investigation into the topic of particle dispersion by forced mixing layers. While part 1 (Martin and Meiburg,[1] hereafter referred to as MM) focused on the effect of the mixing layer alone, we now aim at identifying and quantifying the mechanisms that arise through the interaction of gravity-induced particle settling, with the dispersion process caused by the large-scale structures of the mixing layer. This subject is motivated by both environmental and technical flows. Areas that have been the focus of a good deal of recent research include the atmospheric settling of dust and aerosol particles, as well as the fallout of sediments in rivers and estuaries. In addition, applications involving droplet and particle dispersion abound in the fields of mechanical, chemical, and civil engineering. Examples concern spray combustion and droplet dispersion in the final stages of large turbines. As discussed in MM, within the present study we limit ourselves to small spherical particles with densities much larger than that of the carrier fluid. Furthermore, our investigation targets the dilute regime, in which the interaction among particles, as well as the effect of the particles onto the fluid are negligible. In MM, we had confirmed and extended earlier numerical (Crowe, Gore, and Troutt[2] and Chein and Chung[3]) and experimental (Lazaro and Lasheras[4–6] and Longmire and Eaton[7]) findings of maximum dispersion for those particles with an aerodynamic response time, also called relaxation time, comparable to the characteristic flow time, i.e., a Stokes number of order unity. For the purpose of quantifying the dispersion process, we defined two integral length scales, one of which represents the number of particles that cross the mixing layer, whereas the second one is formed by weighting with the distance. Our simulations showed that, while the number of particles dispersed into the initially unseeded stream does not exhibit a maximum for intermediate Stokes numbers, the distance-weighted dispersion measure does.

By taking gravity into account, we now introduce a third time scale into the problem in the form of a particle settling time. An obvious question that arises concerns the potential modification of the above findings by the inclusion of gravity. It is unknown if optimum dispersion for intermediate Stokes numbers persists as gravity gains importance, and if it does, whether or not the optimally dispersed particle size depends on the strength of gravity. Furthermore, it is of interest to evaluate the effect of the mixing layer on the gravitational settling process. For example, it is unknown if settling is enhanced or delayed by the vortical flow structures. The overall goal is the derivation of quantitative models for the transport of heavy particles in mixing layers under the

 1070-6631/95/7(6)/1241/24/$6.00

added influence of gravity. Such models will have to distinguish between those conditions under which the particle transport from the seeded to the unseeded stream is dominated by gravity and those when the effect of the coherent vortical structures is more important. In order to address the above issues, we have to investigate the coupling mechanisms between settling and dispersion. Some guidance on this matter is provided by the investigations of Stommel[8] and Maxey and Corrsin.[9] These authors study the settling of particles under gravity in doubly periodic cellular flow fields, both with and without particle inertia. They find that particles without inertia can become suspended indefinitely along closed trajectories, while particles with inertia are observed to accumulate in bands and settle out at rates that are usually larger than the gravitational settling rate in a still fluid. For settling in homogeneous turbulence, the findings by Maxey[10] and by Wang and Maxey[11] point toward a larger settling velocity of particles with inertia as well. In particular, Wang and Maxey find increases in the settling velocity up to 50% and larger for particle response times and terminal settling velocities that are comparable to the Kolmogorov scales. However, both particles without inertia and particles with an aerodynamic response time much larger than the flow's integral time scale are expected to settle at the same rate as in still fluid. Manton,[12] on the other hand, had studied the dynamics of an isolated particle in an axisymmetric eddy with a horizontal axis. The observation of approximately closed trajectories and temporary suspension had led this author to argue that the settling rate of heavy particles might be diminished considerably by turbulence. Further interesting findings in this regard are reported by Gañan-Calvo and Lasheras,[13] as well as by Tio, Gañan-Calvo, and Lasheras[14] for more regular, nonturbulent flows. Employing the model of a periodic Stuart vortex array, these authors observe the suspension of heavy particles both above and below the mixing layer for moderate values of gravity, cf. also the findings by McLaughlin.[15] In contrast to the Maxey and Corrsin observations for cellular flow, they report suspension in the mixing layer along open periodic, quasiperiodic, and chaotic trajectories. This example clearly indicates that the dispersion process in a mixing layer under gravity cannot be quantified by linearly superimposing the effect of gravity onto the dispersion by the mixing layer alone, and that instead a careful study of the combined flow field is necessary to elucidate the coupling mechanisms. Comprehensive recent reviews of experimental and computational research on particle dispersion in fluid flows have been given by Crowe, Chung, and Troutt,[16] as well as by Eaton and Fessler.[17]

In most practical applications of particle dispersion by mixing layers, initially only one of the two streams is seeded. If the mean flow direction is horizontal and particle dispersion is to be maximized, the upper stream will be the seeded one. Immediately after the two streams are brought together, the lower stream will contain only very few particles. During this initial transient phase, the growing mixing layer still effectively marks the edge of the seeded flow, i.e., it resides between the seeded and the unseeded stream. However, farther downstream gravity may have caused many particles to enter the lower, initially unseeded stream. For this asymptotic regime of the particle concentration evolution we can hope to derive scaling laws that hold independently of the specific initial conditions.

The paper is organized as follows: In Sec. II, the set of governing equations is briefly reviewed, and the computational approach employed in the present study is outlined. In Sec. III we begin by discussing general aspects of the effects of gravity on particle dispersion in a mixing layer, before presenting specific results for both horizontal and vertical flows, including the influence of vortex pairing. Scaling laws for vortex and gravity dominated regimes are derived and compared with the current computational results. Finally, in Sec. IV we discuss and summarize the main findings, and present some conclusions.

II. GOVERNING EQUATIONS AND DIMENSIONLESS PARAMETERS

The aim of this investigation is to study the spatiotemporal evolution of the concentration of heavy particles, in response to the forcing provided by gravity and the large-scale structures of the growing shear layer. The particles are assumed to be in the dilute regime, in which the evolution of the continuous fluid phase is not affected by the particle concentration. Consequently, the fluid velocities can be obtained independently of the particle motion. In the present study, as in MM, the flow we consider is a temporally evolving two-dimensional mixing layer, whose inviscid evolution can be computed in an efficient way by using a vortex blob technique in conjunction with a fourth-order Runge–Kutta time integration scheme. In this way, the dominant effect of the large-scale vortex structures on the particle dispersion can be captured at a low computational cost. By employing vortex blobs with a Gaussian vorticity distribution, we obtain the unperturbed velocity profile,

$$\mathbf{u}(y) = \tfrac{1}{2}\mathrm{erf}(y), \tag{1}$$

where $\mathrm{erf}(y) = (2/\sqrt{\pi})\int_0^y e^{-\theta^2}\, d\theta$.

Here, as well as below, lengths are rendered dimensionless by referring them to the mixing layer thickness δ, whereas velocities are nondimensionalized by the difference velocity ΔU between the two free streams. To trigger the growth of the coherent structures, a streamwise sinusoidal perturbation of amplitude 0.05 and wavelength L is given to the initial vorticity field. Based on the inviscid linear stability analysis of Michalke[18] for the very similar hyperbolic tangent velocity profile, we choose the wave number to be that of maximum growth, i.e., $\alpha = 2\pi/L = 0.8892$. Further, if a vortex pairing event is to be triggered, the initial vorticity is given a subharmonic perturbation, in addition to the basic disturbance. This subharmonic perturbation is of wavelength *twice* that of the basic one, while its phase is such that its amplitude reaches a maximum midway between the two evolving vortices, so that vortex pairing is obtained. As discussed in MM, we calculate the particle motion from the following truncated version of the full equations given by Maxey and Riley,[19]

$$\frac{d\mathbf{v}_p}{dt} = \frac{1}{\mathrm{St}}\left[\mathbf{u}(\mathbf{x},t)|_{\mathbf{x}=\mathbf{x}_p(t)} - \mathbf{v}_p(t)\right] + \frac{1}{\mathrm{Fr}^2}\,\mathbf{e}_g, \tag{2}$$

$$\frac{d\mathbf{x}_p}{dt}=\mathbf{v}_p, \tag{3}$$

which describe the evolution of particle velocity and location under the effect of inertial, gravitational, and viscous drag forces. Here $\mathbf{u}$ and $\mathbf{v}_p$ represent the fluid and the particle velocity, respectively. Also, $\mathbf{x}_p$ denotes the particle location, where the fluid velocity is obtained by means of an interpolation procedure, as described in detail in MM. The time integration is performed by a fourth-order Runge–Kutta scheme. Gravity has the magnitude g and acts in the direction of the unit vector $\mathbf{e}_g$. We will consider the two cases in which the direction of gravity is parallel or perpendicular to the direction of the free streams. The particle motion is characterized by the dimensionless parameters,

$$\mathrm{St}=\frac{\rho_p d_p^2}{18\mu}\cdot\frac{\Delta U}{\delta}, \quad \mathrm{Fr}=\frac{\Delta U}{\sqrt{\delta g}}.$$

Here ρ_p indicates the density of the particle, d_p refers to its diameter, and μ denotes the fluid viscosity. The Stokes number St expresses the relative importance of particle inertia to viscous drag for the evolution of the particle trajectory. It can be interpreted[2] as the ratio of the particle's aerodynamic response time,

$$\tau_A=\frac{\rho_p d_p^2}{18\mu},$$

and the characteristic flow time,

$$\tau_F=\frac{\delta}{\Delta U}.$$

By including gravity in our investigation, we introduce a third time scale into the problem, namely, the particle setting time,

$$\tau_S=\frac{18\mu\delta}{\rho_p d_p^2 g},$$

which indicates the amount of time it takes a particle falling with its terminal velocity to cover a distance equal to the width of the mixing layer. It is important to appreciate a fundamental difference between τ_A and τ_S: While τ_A expresses the time it takes the particle to respond to *unsteady* forcing by fluctuating fluid velocities, τ_S represents a time scale related to the *steady* forcing by gravity. It characterizes the residence time of the particle in the mixing layer, i.e., the time interval during which the mixing layer can affect the particle in order to enhance or delay settling, or to create nonuniformities in the particle concentration field. The particle motion equation (2) takes gravity into account by means of the Froude number Fr, which is related to the ratio of the particle's settling time to its aerodynamic response time by

$$\tau_S/\tau_A=\mathrm{Fr}^2/\mathrm{St}^2,$$

or, alternatively, to the ratio of the settling time to the characteristic flow time,

$$\tau_S/\tau_F=\mathrm{Fr}^2/\mathrm{St}.$$

The Froude number itself is the square root of the product of the two time scale ratios,

$$\mathrm{Fr}=\left(\frac{\tau_S}{\tau_F}\frac{\tau_A}{\tau_F}\right)^{1/2}.$$

III. RESULTS

A. Preliminary considerations

Before discussing the detailed results of specific calculations, it is helpful to consider some general physical consequences of the nature of the governing system of equations. The first one concerns the importance of the initial conditions for the particle velocity. It is well known that in the absence of gravity the particle relaxation time, i.e., the time after which the particle velocity is not affected by the initial velocity, is proportional to St. By rewriting Eq. (2) for still fluid in terms of $\mathbf{v}_p'(=\mathbf{v}_p-\mathrm{St}/\mathrm{Fr}^2\cdot\mathbf{e}_g)$, i.e., the difference between the instantaneous particle velocity and its terminal settling velocity, we obtain

$$\frac{d\mathbf{v}_p'}{dt}=-\frac{\mathbf{v}_p'}{\mathrm{St}},$$

and when the mixing layer is present,

$$\frac{d\mathbf{v}_p'}{dt}=\frac{\mathbf{u}-\mathbf{v}_p'}{\mathrm{St}}.$$

Hence, even in the presence of gravity the particle relaxation time depends on St only. Fr merely affects the magnitude of the terminal settling velocity.

The second important fact that follows from the governing equations applies to the formation of particle concentration inhomogeneities. In the absence of gravity, the mixing layer has the ability to create quite strong concentration gradients, especially for intermediate values of St. On the other hand, in a still fluid, gravity cannot create concentration gradients, because gravity will uniformly accelerate all the particles without creating any velocity differences among them. Consequently, the only way in which gravity can affect the appearance of concentration inhomogeneities is through the interaction with the effects of the mixing layer.

A final point concerns the modification of the overall settling rate by the mixing layer in the case of initially uniform particle concentration in the entire flow field. In the absence of gravity, the mixing layer vortices will transport just as many particles from the upper stream into the lower one as *vice versa*, so that no net settling will take place. However, this symmetry is broken in the presence of gravity, and it is possible for the mixing layer to interact with the gravity-induced settling in such a way as to hinder or promote it. The suspension effect mentioned above provides an example in this regard.

The latter two of the above remarks emphasize the importance of the nonlinear interaction effects between the mixing-layer-induced particle motion and that caused by gravity. Consequently, we will analyze these interactions in quantitative detail below.

B. Horizontal flow

In the following temporally growing simulations, the flow is from left to right in the upper stream, and from right to left in the lower stream. Gravity points in the direction perpendicular to the free-stream velocity and from the seeded to the unseeded stream. For this configuration, the equations of particle motion are

$$\frac{du_p}{dt}=\frac{1}{\mathrm{St}}(u-u_p), \tag{4}$$

$$\frac{dx_p}{dt}=u_p, \tag{5}$$

$$\frac{dv_p}{dt}=\frac{1}{\mathrm{St}}(v-v_p)-\frac{1}{\mathrm{Fr}^2}, \tag{6}$$

$$\frac{dy_p}{dt}=v_p, \tag{7}$$

where u and v denote the horizontal and vertical fluid velocity components at the particle location. These equations represent a fourth-order, nonlinear dynamical system with two parameters, St and Fr, cf. Gañan-Calvo and Lasheras.[13] The nonlinearity is present in the fluid velocity terms u and v.

In both engineering flows and natural flows, particles are usually seeded in one of the two streams. When the flow is in the horizontal direction, one expects gravity to maximize dispersion, i.e., the particle transport from the seeded to the unseeded stream, if the particles are originally seeded in the upper stream. Hence, in the present study particles are seeded uniformly in the upper stream with an initial velocity equal to the local fluid velocity. We will investigate this issue in more detail below. In the following sections, two types of mixing layer simulations are considered: (i) an evolving mixing layer with only a basic perturbation; and (ii) an evolving mixing layer with both basic and subharmonic perturbations.

1. Basic perturbation only

Here, the initial vorticity field is perturbed with a sinusoidal fundamental wave only. We initially seed the upper stream of the mixing layer by randomly distributing 100 000–200 000 particles and giving them a velocity equal to that of the fluid velocity at the seeded location. The particles are initially seeded between $y=0$ and $y=y_1$, where for most simulations $y_1=5$. However, for some combinations of $\mathrm{St/Fr}^2$, other values of y_1 are employed, so that a steady supply of falling particles is maintained for sufficiently long times. The particles then evolve according to the forcing produced by the vorticity field and by gravity. In order to obtain information on the cross-stream particle concentration profile $c(y)$, the y direction is divided into bins of height $\Delta y=0.05$. The instantaneous number of particles in a bin divided by Δy serves as the particle concentration averaged over one streamwise wavelength. In order to render our results independent of the total number of particles, we will discuss only profiles $c(y)/c_\infty$, where c_∞ is the initial uniform concentration in the seeded free stream.

We begin by giving a phenomenological description of the dispersion and sedimentation process for various parameter combinations, in order to illustrate the physical mechanisms that dominate the different regions of our two-dimensional $\mathrm{St,St/Fr}^2$-parameter plane. Subsequently, we will proceed to a quantitative analysis of the different effects and their interactions.

The first simulation was carried out for $\mathrm{St}=0.1$ and $\mathrm{St/Fr}^2=6.25\times10^{-3}$. From the investigation by MM of particle dispersion in the absence of gravity, we know that for such low values of St, the particles tend to follow the fluid motion, with only a small slip velocity. In order to obtain an estimate for the extent to which gravity affects the particle velocity, it is helpful to remember that $\mathrm{St/Fr}^2$ represents the terminal settling velocity of the particles in still fluid. We recognize that for the present parameter combination, this settling velocity is much smaller than the free-stream velocity of 0.5, so that gravity can be expected to have a small influence. Figure 1 shows the evolution of the isocontours of the vorticity field, along with the locations of 4000–5000 representative particles. To the right of each figure, which for clarity shows two wavelengths of the flow, the streamwise-averaged concentration profiles $c(y)/c_\infty$ are given. Figure 1(a) shows the early stages of the Kelvin–Helmholtz instability at time $t=6$, when weak vortices are beginning to form. By time $t=12$, these vortices have grown much stronger, and only a small amount of vorticity is left in the braid region. In a three-dimensionally evolving flow, this vorticity is known to undergo a reorientation into the direction of extensional strain, thereby forming strong counter-rotating streamwise vortices (Bernal and Roshko,[20] Ashurst and Meiburg,[21] and Lasheras and Choi[22]). The influence of these three-dimensional flow structures on the dispersion process is currently analyzed elsewhere. Figures 1(c) and 1(d) show that, in the absence of a subharmonic perturbation, the vorticity field has reached a nearly steady state by time $t=18$. The particle concentration distribution, however, continues to develop in time, as it is a function of a time integral over the fluid velocities. Figure 1 clearly shows the tendency of small St particles to follow the fluid elements, as long as the influence of gravity is weak. This leads to a point-symmetric transport of the particle-laden fluid and the clear fluid i.e., the particle laden fluid entering the bottom stream and the clear fluid entering the upper stream are symmetric about the center of the vortex. It furthermore results in an antisymmetric $c(y)/c_\infty$ profile with a plateau-like region having a value of approximately 0.5. These symmetries are further enhanced by the temporal nature of our simulation; they would be less pronounced in a spatially growing flow. No significant overshoots appear in the concentration profile, which indicates the absence of regions of high particle concentrations. In this context, it is worthwhile to point out that there are generally two ways in which the flow can promote the development of concentration inhomogeneities: (i) by creating a compressible particle velocity field (cf. MM), i.e., by causing particles to become less concentrated in some regions and more concentrated in others; and (ii) by deforming initially present isocontour lines of the particle concentration field, such as the ones at the lower boundary of the seeded region. For small values of the Stokes numbers, the deformation of preexisting isocontour lines is the predominant mechanism of

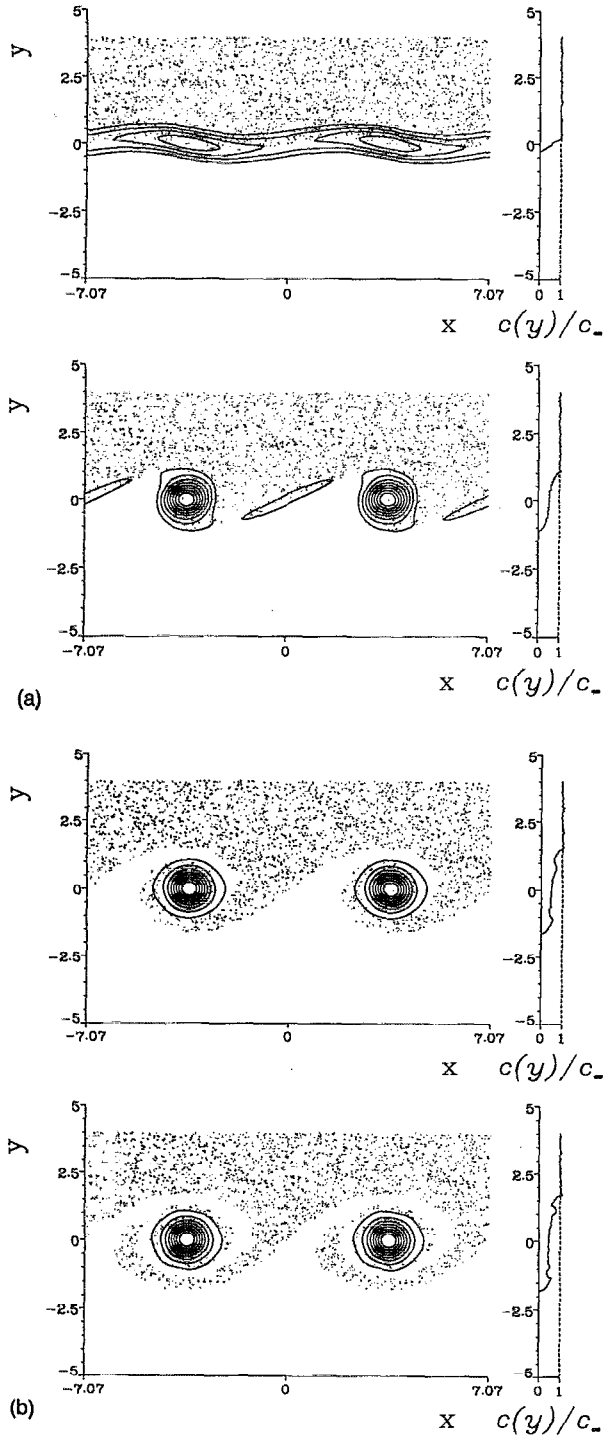

FIG. 1. Mixing layer with a basic perturbation only. Shown are vorticity contours as well as a few thousand representative particle positions for St=0.1 and St/Fr^2=0.006 25. (a) $t=6$; (b) $t=12$; (c) $t=18$; and (d) $t=24$. To the right, the normalized concentration profile averaged over one streamwise wavelength is given. The particles tend to follow the fluid, even in the presence of weak gravity. The point symmetry between the particle-laden fluid and the clear fluid is reflected in the plateau region of the concentration profile.

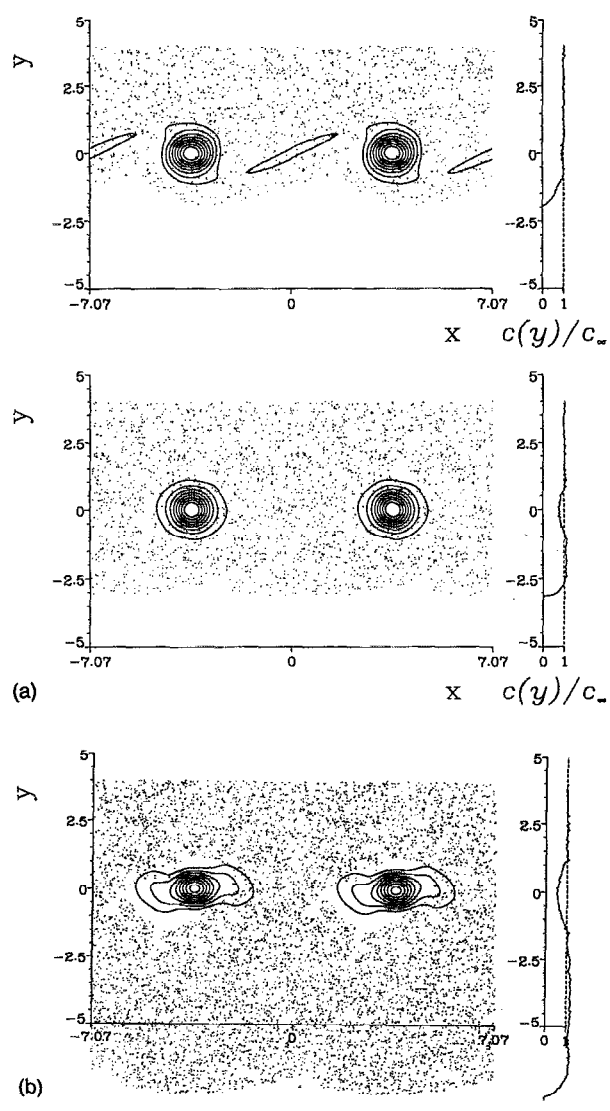

FIG. 2. Particle positions and concentration for St=0.1 and St/Fr^2=0.123. (a) $t=12$; (b) $t=24$; and (c) $t=60$. The particle motion is dominated by gravity. The reduced concentration in the region of the mixing layer is due to the void regions near the vortex cores. It indicates enhanced particle settling as a result of the presence of the mixing layer. For long times, an asymptotic concentration field develops in which the concentration is unity above ($y>1.5$) and below ($y<-1.5$) the mixing layer region.

producing concentration inhomogeneities. As we will see below, for larger Stokes numbers the compressibility effect is the predominant mechanism.

Next we discuss a simulation for St=0.1 and St/Fr^2=0.123; cf. Fig. 2. Compared to the previous case, the ratio of particle response time to characteristic flow time has not changed. However, the ratio of characteristic flow time to particle settling time scale has increased by a factor of almost 20, so that gravity is expected to dominate the particle dynamics to a much larger extent than before. As a result, the above symmetry properties of the particle concentration field do not appear. Instead, the particles settle in a nearly uniform fashion, again without forming regions of high concentrations. The evolving mixing layer does not have enough time to pull strands of clear fluid up into the seeded stream, or to eject bands of particle carrying fluid into the unseeded stream. Only near the upstream edge of the vortices, a region of reduced particle concentration forms as a result of centrifugal effects. This demonstrates that even for the present

parameter combination, the fluid velocity still has the ability to create slight nonuniformities in the particle concentration field by causing small compressibility effects in the particle velocity field. The influence of the fluid velocities on the particle dynamics is furthermore reflected in the deformation of the lower boundary of the particle-laden region, which initially was located at $y=0$. Under the influence of gravity only, this boundary would remain horizontal for all times. By time $t=24$, the particle concentration in the lower stream just below the mixing layer slightly exceeds unity, which is due to the initial transient evolution of the fluid and particle velocities. In the absence of permanent particle suspension, and for a steady-state vorticity field, an asymptotic particle concentration field has to develop with $c(y)/c_\infty=1$ at some distance above and below the mixing layer, as can be seen for $t=60$ in the region $-2<y<-1.5$. For the present parameter combination, on average, $c(y)/c_\infty<1$ between these regions, which indicates that the particle settling is accelerated by the existence of the mixing layer. Since both Stommel,[8] as well as Maxey and Corrsin,[9] showed that particles without inertia settling under gravity create an incompressible particle velocity field, we have to conclude that even for such small values of St as 0.1, the particles have enough inertia for compressibility effects in the particle velocity field to be generated.

The simulation shown in Fig. 3 tracks particles with St=3 and $\mathrm{St/Fr^2}=6.25\times10^{-3}$. The ratio of characteristic flow time and settling time is the same as in the calculation of Fig. 1. However, the ratio of the particle response time to the characteristic flow time is now larger by a factor of 30. In the absence of gravity, we know that these St values lead to the ejection of particles from the vortex centers, a tendency that is reflected in the present simulation as well. The areas near the vortex centers become depleted of particles, and bands of high particle concentration form in the braid region by time $t=18$. Furthermore, we observe the evolution of an overshoot in the concentration profile just above the mixing layer, initially between $y=1$ and $y=1.5$. The maximum of this overshoot grows with time while moving to slightly larger y values. Simultaneously, the high concentration bands in the braid region become weaker. The later stages of the calculation suggest that for this particular parameter concentration, the band formation is a purely transient process, whereas soon most of the particles become suspended above the mixing layer. This situation reflects the identification of a suspension mode for heavy particles settling under the influence of moderate gravity by Gañan-Calvo and Lasheras,[13] as well as by Tio, Gañan-Calvo, and Lasheras.[14] We will investigate below to what extent this suspension mechanism remains important in the presence of a vortex pairing event.

The calculations shown in Figs. 1 and 3 allow us to draw some preliminary conclusions about the settling of particles through a mixing layer for weak gravity, i.e., for $\mathrm{St/Fr^2}\ll1$. Under these circumstances, the particles will spend a fairly long time in or near the mixing layer, and the unsteady fluid velocity fluctuations they see are much larger than their terminal settling velocity. For $\mathrm{St}\ll1$ the particles follow the fluid elements closely, with a small slip velocity due to gravity. Consequently, no strong compressibility effects can be

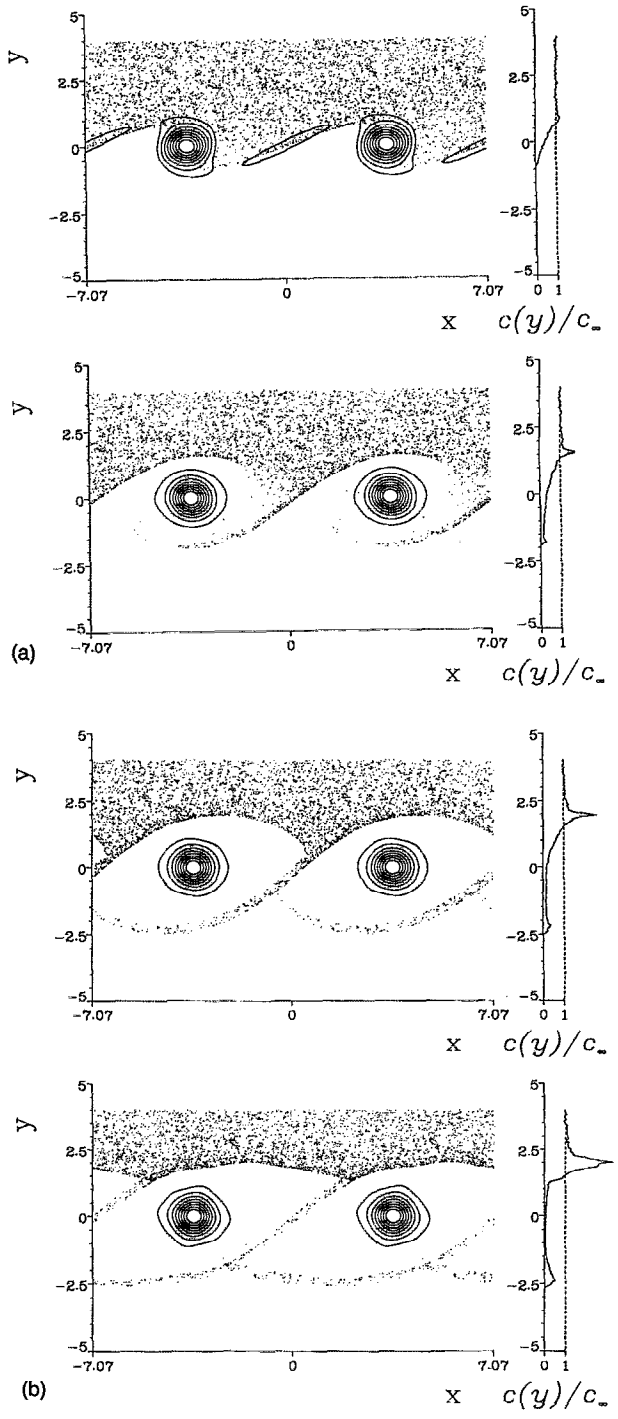

FIG. 3. Particle positions and concentration for St=3.0 and $\mathrm{St/Fr^2}=0.006\,25$. (a) $t=12$; (b) $t=18$; (c) $t=24$; and (d) $t=30$. The increased particle inertia leads to their ejection from the vortex cores, upon which they accumulate in bands in the braid region. Weak gravity permits suspension to occur for the present parameters, which leads to the growing overshoot in the concentration profile.

created in the particle velocity field. For large enough values of Fr, suspension will be possible in this low terminal velocity regime, provided the particles have sufficient inertia to be able to bounce from one vortex to the next, a prerequisite for suspension along open trajectories as shown by Gañan-Calvo and Lasheras.[13] If $\mathrm{St}\simeq1$, the particles' aerodynamic response

time is comparable to the characteristic fluid time, so that for the present small settling velocities, the mixing layer vortices will be able to affect the particle velocities and create particle concentration nonuniformities. Suspension is again possible under these circumstances for sufficiently large values Fr. For St$\gg$1, on the other hand, we expect the slowly settling particles to be almost unaffected by the vortical structures, due to their large inertia. In this case, the particle path will for a time interval $O(\mathrm{St})$ be dominated by the initial condition for the particle velocity. The initial particle velocity, and the amount of time it takes the particle to reach the mixing layer, will be important in deciding whether the particle will settle through the mixing layer or become suspended. If the parameter values and initial conditions are such that suspension occurs, the mixing layer can represent an effective barrier to the settling particles. The result will be an upper free stream out of which the particles settle into a high concentration boundary layer just above the mixing layer. The lower stream will remain largely void of particles under these conditions.

We conclude the phenomenological part of our description by discussing the simulation shown in Fig. 4 of particle settling for St=3 and $\mathrm{St/Fr^2}=0.333$. The ratio of particle response time to characteristic flow time is the same as before, however, the ratio of characteristic flow time to settling time has increased by a factor of approximately 50. The resulting increase in the importance of gravity makes permanent suspension impossible. Even though an overshoot still forms in the concentration profile above the mixing layer, this overshoot reaches a statistically steady state, reflecting the fact that after a transient period just as many particles enter from above as leave below. The overshoot furthermore indicates the tendency of the mixing layer to slow down the settling process of St=3 particles, in contrast to particles of St=0.1, for which we observed accelerated settling in Fig. 2. The increase in St furthermore allows much more pronounced inhomogeneities in the particle concentration field to form. Their most prominent feature is a band-like structure, which begins very near the vortex center and extends far into the lower free stream. These bands of high particle concentrations are separated by regions of fluid nearly devoid of particles. They persist in the lower stream, as the particle velocity components asymptotically approach -0.5 in the horizontal and $-\mathrm{St/Fr^2}$ in the vertical direction. As a result, the asymptotic angle that the parallel bands form with the horizontal axis [Fig. 4(c)] is given by

$$\tan\alpha=\frac{v_p}{u_p}=\frac{2\ \mathrm{St}}{\mathrm{Fr}^2}. \tag{8}$$

For the distance between two adjacent bands, we obtain

$$d=L\ \sin\alpha=L\ \sin\left[\tan^{-1}\left(\frac{2\ \mathrm{St}}{\mathrm{Fr}^2}\right)\right]. \tag{9}$$

For the case without gravity, a scaling law was derived in MM for the accumulation of particles in the braid region connecting the coherent vortices. It shows that this accumulation in bands near the free stagnation points proceeds in an optimal fashion for St=1. In the following, we will extend this scaling law to include gravity.

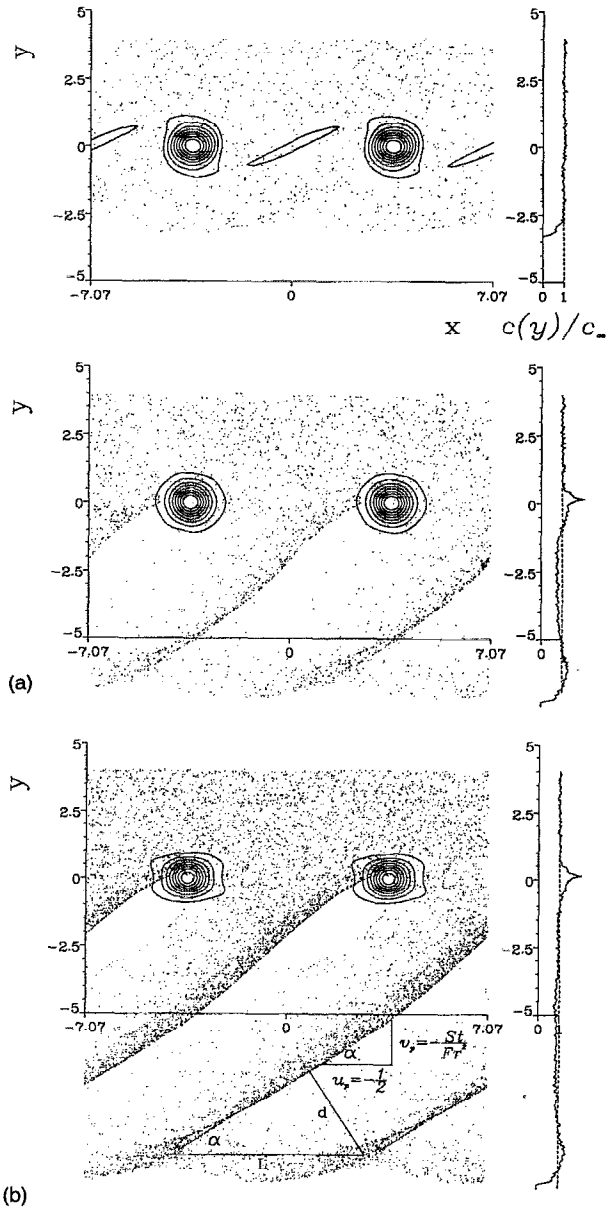

FIG. 4. Particle positions and concentration for St=3.0 and $\mathrm{St/Fr^2}=0.33$. (a) $t=12$; (b) $t=24$; and (c) $t=36$. The interaction of particle ejection from the vortex cores, accumulation in the braids, and gravity leads to particle settling in the form of bands. The overshoot in the concentration profile indicates the tendency toward particle suspension. However, the overshoot saturates, as permanent suspension does not occur. The scaling laws for the asymptotic angle of the bands and the distance between them are shown in frame (c).

The particle behavior in the braid region can be studied analytically by representing the flow field as a time-independent row of point vortices located at $x=,\ldots,-3L/2, -L/2, L/2, 3L/2,\ldots$, and $y=0$, and by subsequently linearizing near the free stagnation point at the origin. If for simplicity we take $L=2\pi$, which is close to the wavelength employed in the numerical simulation, this linearized velocity field is given by

$$u=ay,\quad v=ax,$$

where the strain rate a for the present case has the value $\frac{1}{4}$. The equations governing the particle motion are

$$\frac{d^2x}{dt^2}=\frac{1}{\mathrm{St}}\left(ay-\frac{dx}{dt}\right), \tag{10}$$

$$\frac{d^2y}{dt^2}=\frac{1}{\mathrm{St}}\left(ax-\frac{dy}{dt}\right)-\frac{1}{\mathrm{Fr}^2}. \tag{11}$$

Through a coordinate transformation the above equations can be decoupled. Let $\xi=(x+y)/\sqrt{2}$ and $\eta=(y-x)/\sqrt{2}$. The ξ axis forms an angle $\theta=45°$ with the x axis, while the η axis is at an angle $\alpha=135°$ (Fig. 5). On adding $1/\sqrt{2}$ times Eq. (10) and $1/\sqrt{2}$ times Eq. (11),

$$\frac{d^2\xi}{dt^2}+\frac{1}{\mathrm{St}}\frac{d\xi}{dt}=\frac{a}{\mathrm{St}}\xi-\frac{1}{\sqrt{2}\mathrm{Fr}^2},$$

and on subtracting $1/\sqrt{2}$ times Eq. (10) from $1/\sqrt{2}$ times Eq. (11),

$$\frac{d^2\eta}{dt^2}+\frac{1}{\mathrm{St}}\frac{d\eta}{dt}=-\frac{a}{\mathrm{St}}\eta-\frac{1}{\sqrt{2}\mathrm{Fr}^2}.$$

The solution for the η equation is

$$\eta=c_1e^{\lambda_1 t}+c_2e^{\lambda_2 t}-\frac{\mathrm{St}}{a\sqrt{2}\mathrm{Fr}^2},$$

$$\lambda_{1,2}=\frac{-1\pm\sqrt{1-4a\mathrm{St}}}{2\,\mathrm{St}},$$

where c_i is of the form $k_{i1}(\mathrm{St}/\mathrm{Fr}^2)+k_{i2}\,\eta(t=0)+k_{i3}\,\dot{\eta}(t=0)$ and k_{ij} depends on St. Clearly, both λ_1 and λ_2 have negative real parts and the particle asymptotically approaches $\eta=-\mathrm{St}/a\sqrt{2}\mathrm{Fr}^2$ as $t\to\infty$, instead of $\eta=0$ in the case without gravity. Just as in the absence of gravity, the system is critically damped for St=1, so that the same particles experience optimal accumulation.

In order to demonstrate the above-mentioned effects, the trajectories of particles in the linearized flow field are plotted for various values of St and for the settling velocities $\mathrm{St}/\mathrm{Fr}^2$ equal to zero (Fig. 5) and 0.5 (Fig. 6). Shown in each figure are the particle trajectories for St values of 0.1, 1, and 5 (solid lines), along with the streamlines of the linearized velocity field (dotted lines). The fourth frame in Fig. 6 compares the streamlines of this velocity field (dotted lines) with those of the modified velocity field $v'=v-\mathrm{St}/\mathrm{Fr}^2$ (solid lines). It is the separatrix of this modified velocity field that serves as the attractor for the particles. In other words, the location of the band is shifted along the $-\eta$ axis by a distance equal to $\mathrm{St}/a\sqrt{2}\mathrm{Fr}^2$, compared to the case without gravity. These figures confirm that, for constant settling velocity, the accumulation rate of the particles is highest for St=1, due to the critical damping. For lower values of St, the particle motion is overdamped, which leads to the widening of the band. For larger values of St, the system is underdamped, thereby causing the particles to overshoot, which, in turn also widens the band. When the settling velocity is increased for the same value of St, the particle residence time near the stagnation point decreases, so that the flow has less time to concentrate the particles. As a result, the width of the bands again increases. In the limit as Fr→0, gravity dominates, and the particles fall down uniformly without accumulating in bands.

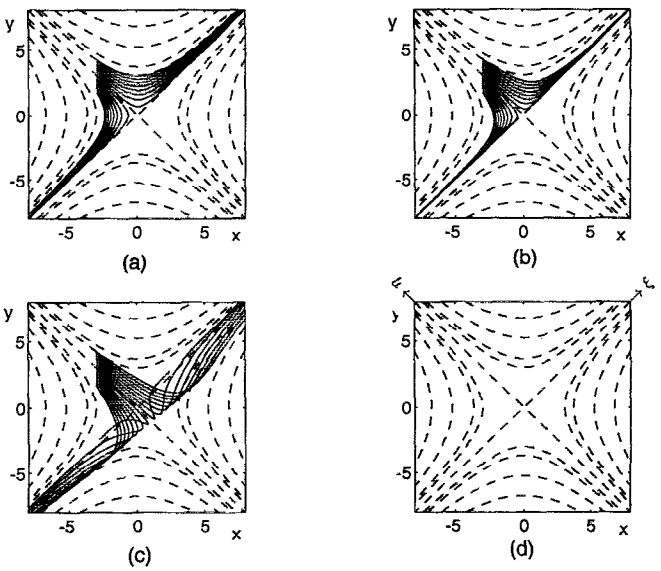

FIG. 5. Particle trajectories (solid lines) in the linearized flow field near the free stagnation point for the case without gravity. Shown by dashed lines is the streamfunction. (a) St=0.1; (b) St=1; (c) St=5; and (d) streamlines and transformed coordinate axes for the linearized velocity field. For St=1, the particles display optimal focusing along the ξ axis. The particle motion is underdamped for St>1, critically damped for St=1, and overdamped for St<1.

While it was shown in MM that St~1 leads to optimal particle accumulation by the strain field in the absence of gravity, the above analysis demonstrates that this finding

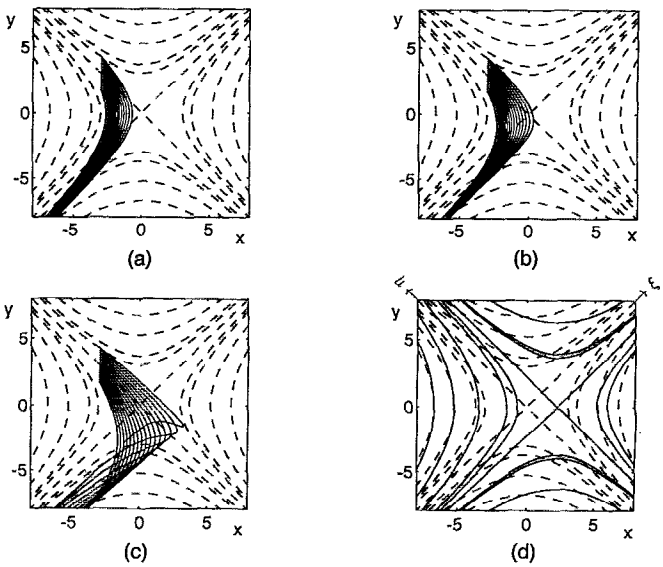

FIG. 6. Particle trajectories (solid lines) and streamfunction (dashed lines) in the linearized flow field for $\mathrm{St}/\mathrm{Fr}^2=0.5$; (a) St=0.1; (b) St=1; (c) St=5; and (d) streamfunction for the linearized flow field (dashed lines) along and for the modified velocity field (solid lines); Increasing gravity shifts the line of accumulation (ξ axis) to the right and widens the bands (compare Fig. 5). The damping characteristics remain unchanged.

translates to situations with gravity as well. In the following, we conduct a similar linear analysis for the core region of the vortices, in order to investigate if the ejection mechanism reaches an optimum for intermediate values of St as well. For this purpose, we linearize the flow field around the vortex center, where we assume that the velocity field approaches that of a solid body vortex. If we denote the local vorticity by Ω_0, the linearized fluid velocity components are

$$u=\frac{\Omega_0}{2}y, \quad v=-\frac{\Omega_0}{2}x. \tag{12}$$

The particle motion, in the absence of gravity, is governed by

$$\ddot{x}=\frac{1}{\mathrm{St}}\left(\frac{\Omega_0}{2}y-\dot{x}\right),$$

$$\ddot{y}=\frac{1}{\mathrm{St}}\left(-\frac{\Omega_0}{2}x-\dot{y}\right),$$

which has a solution

$$x=c_1e^{\lambda_1 t}+c_2e^{\lambda_2 t}+c_3e^{\lambda_3 t}+c_4e^{\lambda_4 t},$$

$$y=i(c_1e^{\lambda_1 t}-c_2e^{\lambda_2 t}+c_3e^{\lambda_3 t}-c_4e^{\lambda_4 t}),$$

$$\lambda_{1-4}=\frac{-1\pm\sqrt{1\pm 2i\Omega_0\,\mathrm{St}}}{2\,\mathrm{St}}.$$

The largest real part of the eigenvalues λ_i is given by

$$\mathrm{Re}(\lambda)_{\max}=\frac{-1+\sqrt{(1+\sqrt{1+4\Omega_0^2\mathrm{St}^2})/2}}{2\,\mathrm{St}}.$$

For the present mixing layer, the maximum vorticity of the unperturbed velocity profile [Eq. (1)] is $1/\sqrt{\pi}$. For the two-dimensional inviscid evolution considered here, this value continues to represent the maximum vorticity in the flow field (if the amplitude of the initial perturbation is negligible), i.e., the vorticity level at the vortex center. For this Ω_0, the real part of the positive eigenvalue is maximized when St≈3.5. In other words, particles with this Stokes numbers are thrown out of the vortex core region at an optimal rate. It should be mentioned that for the solid body vortex, a more appropriate definition of the Stokes number should use $2/\Omega_0$ as the fluid time scale, rather than $\delta/\Delta U$. Ejection from the vortex is then maximized when this modified Stokes number has a value of 1. Some of the particles experiencing optimal ejection enter the unseeded stream directly, while some others move toward the stagnation point streamline, where they are optimally focused by the strain field. Combined, the two effects of optimal particle ejection and optimal particle focusing maximize dispersion for intermediate St values. The ejection process becomes clearer when the particle equation is cast in polar coordinates,

$$\ddot{r}=-\frac{\dot{r}}{\mathrm{St}}+r\omega^2, \tag{13}$$

$$\dot{\omega}+2\frac{\dot{r}}{r}\omega=\frac{1}{\mathrm{St}}\left(-\frac{\Omega_0}{2}-\omega\right), \tag{14}$$

where r is the radius and ω is the angular velocity of the particle. In Eq. (13), the first term on the right-hand side

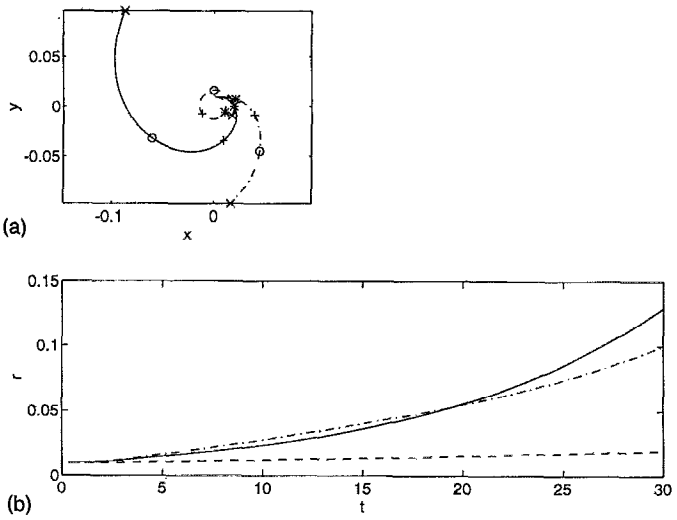

FIG. 7. Particle trajectories (a) and the distance from the center for various times (b) in a linearized flow field that approximates the vortex core as a solid body vortex; ---, St=0.3; —, St=3.5, and -·-, St=20. By $t=20$, optimal ejection is seen for St=3.5 because, at this value of St, the difference between the centrifugal force per unit mass and the opposing drag is maximized. The effect of the particular initial conditions chosen here prevents St=3.5 from showing optimality for early times.

corresponds to the drag force while the second term is proportional to the centrifugal force per unit mass. Both the centrifugal force and the opposing drag force decrease uniformly as St increases. However, the resultant force, which is the vectorial sum of these two forces, is maximized for intermediate values of St, which results in optimizing dispersion. For low values of St, the drag term in the radial equation strongly reduces any radial acceleration by forcing the particle to follow the fluid motion closely, thereby preventing it from quickly moving to larger radii. For large values of St, the fluid is unable to impart a significant angular velocity on the particle, which, in turn, prevents the generation of strong centrifugal forces that would accelerate the particle toward larger radii. At the optimal value of St (Fig. 7), the fluid has just enough viscosity to spin the particle up to significant angular velocities without suppressing the resulting radial motion. Consequently, the centrifugal force accelerates the particle toward larger radii, where it will acquire larger circumferential velocities, which, in turn, will lead to larger centrifugal forces, etc.

The calculations described in Figs. 2 ($\mathrm{St/Fr^2}=0.123$) and 4 ($\mathrm{St/Fr^2}=0.33$) indicate some general trends for particle settling under fairly strong gravity, i.e., $\mathrm{St/Fr^2}\sim O(1)$. Under these conditions, suspension above the mixing layer will not be possible. Furthermore, the particles settle through the mixing layer quite rapidly, so that the capability of the nonuniform velocity field to create particle concentration inhomogeneities will be limited. For small values of St, such inhomogeneities can only be generated through the deformation of isoconcentration lines already present at earlier times. For intermediate values of St, high concentration particle bands form, which become less sharp as the importance of gravity increases. For St≫1, inhomogeneities will not form, except as a direct consequence of the initial particle veloci-

ties. As the importance of gravity increases further, i.e., for $St/Fr^2 \gg 1$, concentration inhomogeneities will become less pronounced for all values of St, as the time interval during which the vortical structures can affect the particle dynamics becomes even shorter.

In order to quantify the effect of St and Fr on concentrating the particles along preferential paths, we analyze the root mean square (RMS) of the particle concentration field. For this purpose, we divide the entire flow field into $M \times N$ rectangular bins, within which the number of particles $n_{i,j}$, $i=1,M$, and $j=1,N$ is counted. Care has to be taken in selecting appropriate values for M and N. For the sake of resolving the details of the particle concentration field, we would like the bins to be as small as possible. On the other hand, the smaller the bins, the fewer particles are located within each bin, so that the relative fluctuations due to the random seeding increase. However, there is a range for M and N in which the structure of the concentration field is adequately resolved, and the random fluctuations are much smaller than those due to the effect of the flow field structure on the particle concentration field. In order to stay in this range, M was typically taken to be 20 per wavelength, while N was selected, such that there are 5 bins per unit length in the cross-stream direction. The streamwise-averaged number of particles $\bar{n}_j$ in the row of bins centered around y_j is

$$\bar{n}_j = \frac{\sum_{i=1}^{M} n_{i,j}}{M}. \tag{15}$$

The streamwise RMS value n_j' of the number of particles at this y location is then

$$n_j' = \sqrt{\frac{\sum_{i=1}^{M} (n_{i,j} - \bar{n}_j)^2}{M}}. \tag{16}$$

In order to render the results independent of the total number of particles, we divide this number by the average initial number of particles per bin, n_0, in the seeded stream. Here n_j'/n_0 is plotted in Figs. 8 ($t=18$) and 9 ($t=30$) for different values of St and Fr. Larger values of n_j'/n_0 indicate more pronounced concentration inhomogeneities. The data for the seeded free stream indicate the level of the RMS fluctuations that is due to the initial random seeding. As seen above, for $St=0.1$ and $St/Fr^2=0.006\,25$ the particles tend to move with the fluid, and gravity is not strong enough to alter the particle paths significantly. The nearly point-symmetric rollup of clear fluid, in which the concentration remains near zero, and particle-laden fluid, in which the concentration remains near unity, leads us to expect RMS values of the particle concentration field on the order of, but not larger than, one-half, which is confirmed by Fig. 8(a) for the region containing the coherent vortices. As St/Fr^2 is increased to 0.123, the particles fall more rapidly. Simultaneously, they experience a slight acceleration away from the vortex cores. Initially this leads only to a slight decrease of the concentration in those regions, and consequently to lower RMS values on the order of one-third in the vortical region. By time $t=30$, however, the RMS values have increased to about 0.5. The second peak in the RMS values for lower y values is due to the deformation of the initially horizontal lower boundary of the

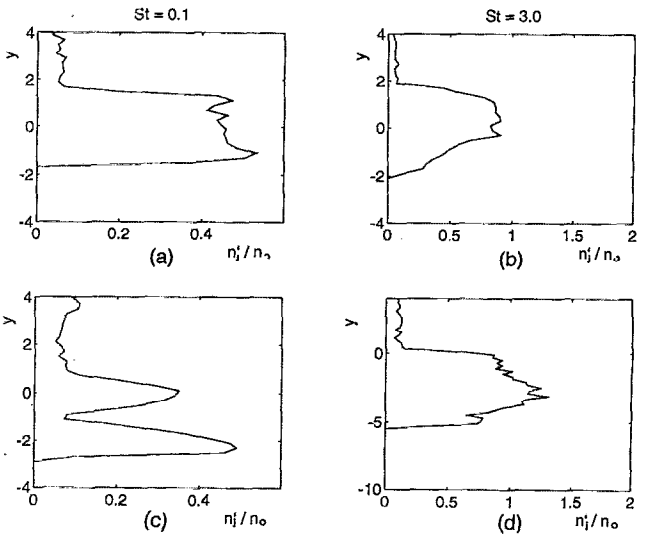

FIG. 8. Root mean square of the particle concentration field along lines $y=$const, at $t=18$; (a) $St=0.1$, $St/Fr^2=0.006\,25$; (b) $St=3$, $St/Fr^2=0.006\,25$; (c) $St=0.1$, $St/Fr^2=0.123$; and (d) $St=3$, $St/Fr^2=0.33$. For $St=0.1$, the particles follow the fluid, and the local concentration is either zero or unity. Consequently, the RMS value cannot exceed 0.5. For $St=3$, regions of strong particle accumulation form, resulting in larger RMS values. The RMS levels in the seeded free stream indicate the fluctuations due to the random seeding.

seeded region. Here the alternating presence of clear fluid and fluid with a particle concentration near unity again leads to RMS values of about 0.5.

For $St=3$, we observe considerably larger peak rms values, indicating that for these higher Stokes numbers the fluid velocity field creates more pronounced accumulations of particles. The graph for $St/Fr^2=0.006\,25$ and $t=30$ [Fig. 9(b)] reflects the suspension of the particles in a wavy region above the vortices, whereas the large RMS values for $St/Fr^2=0.333$ are due to the formation of the bands. In agreement with our observations from the calculations described above, these data show that the maximum RMS values depend more on St than on St/Fr^2, indicating that the ability of the particles to accumulate in certain regions is mostly a function of St. However, it is the interaction between the fluid velocity field and gravity that determines the nature of this accumulation, i.e., whether there will be suspension or settling in bands, for example. In addition, this interaction determines whether gravity amplifies or attenuates the concentration in the accumulation zones. As discussed earlier, increasing the relative strength of gravity has the effect of distributing the particles over a larger region, which is reflected in the widening of the bands. Despite this widening, increasing gravity can amplify the rms values by bringing more particles into the strain field region, where the mixing layer accumulates the particles in bands [compare Fig. 8(d) with 8(b)].

The above simulations indicate the following tendencies of the settling process: Particle concentration inhomogeneities can form for weak gravity as a result of suspension, and for intermediate values of St and moderate strengths of gravity in the form of concentrated particle bands. In general, for these bands to form the flow field needs to be able to affect

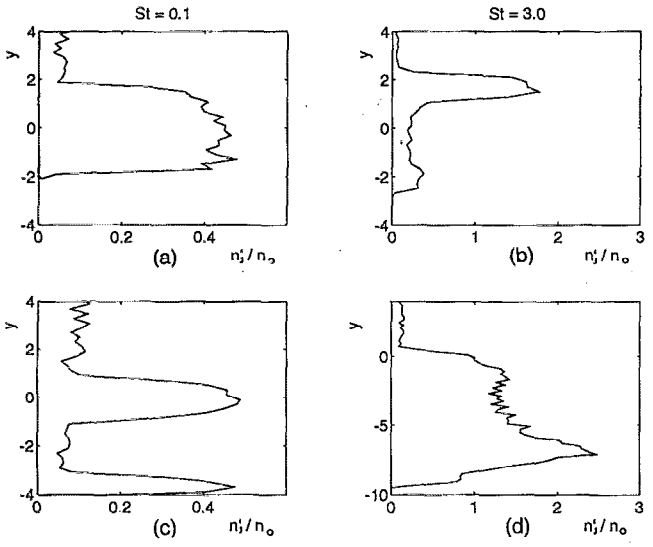

FIG. 9. Root mean square of the particle concentration field along lines y=const at t=30; (a) St=0.1, St/Fr^2=0.006 25; (b) St=3, St/Fr^2=0.006 25; (c) St=0.1, St/Fr^2=0.123; and (d) St=3, St/Fr^2=0.33. While for weak gravity and St=3, suspension leads to large RMS values in the upper, seeded free stream, for strong gravity the settling bands result in large rms values in the lower stream.

the particles over sufficiently long times, i.e., for a given value of Fr, St has to be sufficiently small. On the other hand, the formation of the bands requires significant relative velocities between fluid and particles, i.e., sufficiently large values of St. As a result, the formation of the bands is optimized for intermediate St values. For large St, the situation depends strongly on the initial particle velocities.

We now proceed to analyze the above simulations, as well as many more for other combinations of St and Fr, in a more quantitative fashion. For this purpose, we employ the same two integral scales as in MM. The first one is the displacement thickness $\delta_d(t)$, which gives a measure of the number of particles below $y=0$, i.e., in the initially unseeded stream. It is defined as

$$\delta_d(t)=\int_{-\infty}^{0}\frac{c(y,t)}{c_\infty}\,dy. \tag{17}$$

The weighted displacement thickness $\delta_\chi(t)$, on the other hand, is formed by weighting with the distance of penetration,

$$\delta_\chi(t)=\int_{-\infty}^{0}|y|\frac{c(y,t)}{c_\infty}\,dy. \tag{18}$$

The ratio of these two thicknesses $\delta_\chi(t)/\delta_d(t)$ gives the average distance of penetration $\bar{y}(t)$. We will compare these two thicknesses with those effected by gravity alone, acting on particles initially at rest in still fluid. For this special case, the governing equations are linear and analytical expressions can be found for the instantaneous velocity $\mathbf{v}_p$, displacement thickness δ_{dg} and weighted displacement thickness $\delta_{\chi g}$:

$$\mathbf{v}_p=(1-e^{-t/\mathrm{St}})\frac{\mathrm{St}}{\mathrm{Fr}^2}\,\mathbf{e}_g, \tag{19}$$

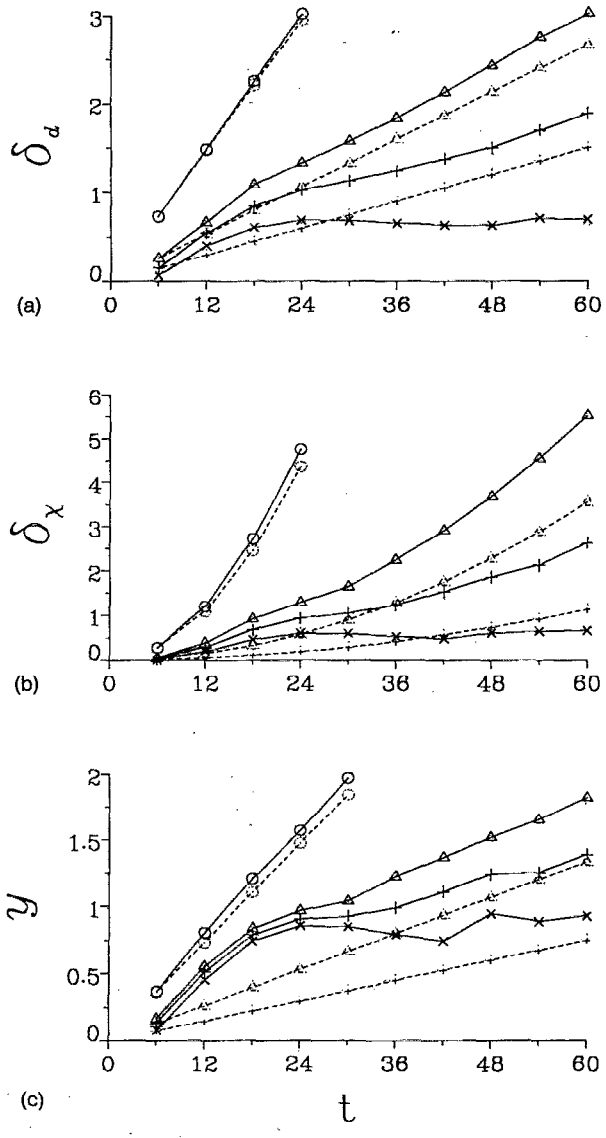

FIG. 10. (a) Displacement thickness, (b) weighted displacement thickness, and (c) average distance of penetration for St=0.1; ×, Fr=∞; +, Fr=2; △, Fr=1.5; and ○, Fr=0.9. Solid lines indicate the case where both the mixing layer and gravity are present, while dashed lines are for settling in still fluid. As gravity increases, both the number of particles, their weighted displacement thickness, and the average distance by which they penetrate the bottom layer increase. All three dispersion measures are enhanced by the presence of the mixing layer. Notice the saturation of the contribution by the mixing layer alone (× line) for $t>20$.

$$\delta_{dg}=\frac{\mathrm{St}^2}{\mathrm{Fr}^2}(e^{-t/\mathrm{St}}-1)+\frac{\mathrm{St}}{\mathrm{Fr}^2}\,t, \tag{20}$$

$$\delta_{\chi g}=\frac{\delta_{dg}^2}{2}. \tag{21}$$

As $t\to\infty$, $\mathbf{v}_p\to(\mathrm{St}/\mathrm{Fr}^2\mathbf{e}_g)$, which is the terminal velocity.

For St=0.1, Fig. 10 compares these two integral scales, as well as the average distance of penetration, for settling in still fluid (dashed line) with settling through a mixing layer (solid line). Fr varies from strong gravity (Fr=0.9) to no gravity (Fr=∞). For this small St case, the number of particles crossing the x axis departs significantly from the result

for settling in still fluid, particularly for early times and large values of Fr; cf. Fig. 10(a). During these early stages and for a moderate strength of gravity, the strands of particle-laden fluid that are pulled across the x axis as a result of the vortical motion represent the main mechanism by which particles enter the lower stream. However, beyond $t \simeq 20$, the mixing layer contribution saturates due to the absence of a subharmonic perturbation, and the settling of the particles becomes increasingly dominated by gravity. The number of particles entering the lower stream increases uniformly with gravity.

The weighted displacement thickness shows very similar tendencies; cf. Fig. 10(b): For moderate values of gravity, it is also initially dominated by the mixing layer contribution. At later times, after saturation of the mixing layer, gravity becomes the dominant factor, causing particles to cross into the lower stream. The dominance of the mixing layer during the early stages is reflected in the average displacement plot as well; cf. Fig. 10(c). Here, the oscillatory behavior for weak gravity and large times results from the particle bands' wrapping around the vortical structures. In summary, for the small value St=0.1, the presence of the mixing layer leads to an increase in all three measures of the particle settling process for all values of Fr. This is in agreement with the dip in the $c(y)/c_\infty$ profile observed to develop in the vortical region for St=0.1 and St/Fr^2=0.123 (Fig. 2).

The quantitative results for St=1 reflect the increasing importance of the particles' inertia (Fig. 11). It can be seen that both integral scales increase monotonically with decreasing Fr. For the mixing layer alone, the displacement thickness, i.e., the number of particles ejected into the opposite stream, increases until about $t=20$ and stays constant thereafter. For relatively weak gravity, Fr=5, the presence of the mixing layer initially enhances the number of ejected particles, but for long times lowers it. This reflects the tendency of the vortices to suspend the settling particles. However, even at long times, for Fr=5, particles keep entering the lower stream, indicating that the mixing layer has not become an impenetrable barrier to the particles. For cases with stronger gravity, the mixing layer makes no significant contribution to the number of settling particles, and the displacement thickness is nearly identical to that caused by gravity alone. It should be pointed out that, in contrast to particle suspension, particle settling in bands does not affect the integral scales. The band formation will, however, be reflected in the RMS characteristics of the concentration field.

For the weighted displacement thickness the picture looks somewhat different [Fig. 11(b)]: Here the presence of the mixing layer consistently leads to an increase compared to settling under gravity alone. As gravity becomes more important, the increase first becomes more pronounced, but then levels off. This behavior indicates that while the mixing layer does not lead to a significant increase in the *number* of particles for St=1, it ejects them *farther* into the lower stream. The plot of the average penetration distance [Fig. 11(c)] confirms this effect of the presence of the mixing layer, for all times and Fr values.

For St=3, the calculations described above in detail

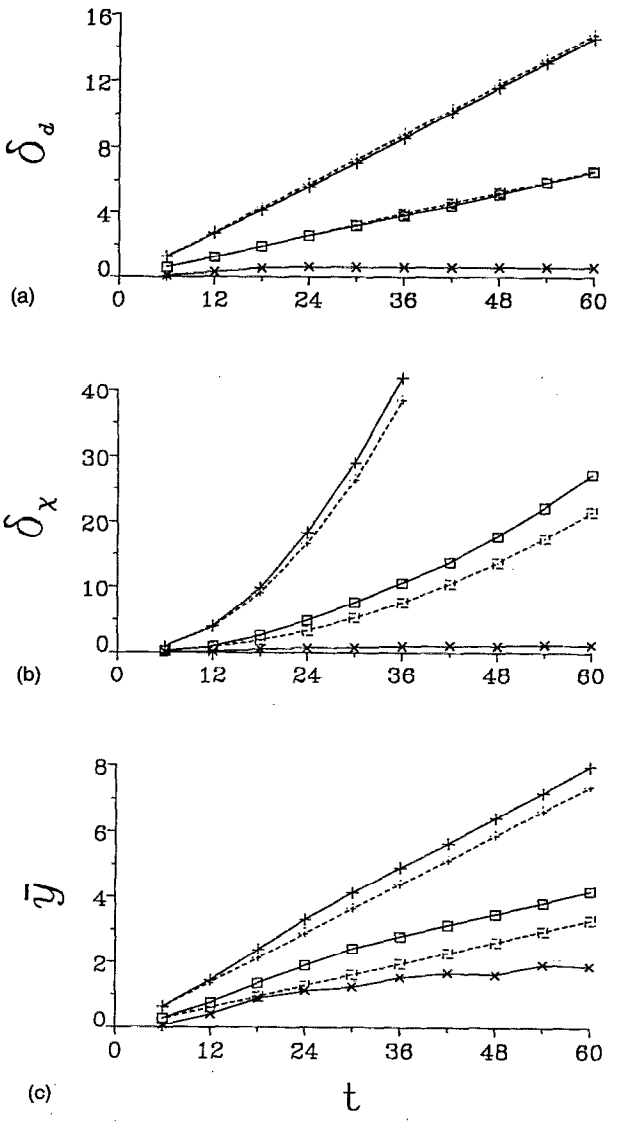

FIG. 11. (a) Displacement thickness, (b) weighted displacement thickness, and (c) average distance of penetration for St=1; ×, Fr=∞; □, Fr=3; and +, Fr=2; Solid lines denote the case of settling through the mixing layer, while dashed lines indicate settling in still fluid under gravity. For weak gravity (Fr=5), the mixing layer initially enhances the number of particles, but later lowers it by suspending them in the seeded stream. For strong gravity, the mixing layer slightly decreases the number of dispersed particles, but increases their distance of penetration.

demonstrate the existence of the suspension mode, a mechanism that is confirmed by the quantitative data shown in Fig. 12. For Fr=8, we find that the number of particles in the lower stream stays approximately constant after $t=24$, indicating that the mixing layer has become an impenetrable barrier to the particles, which, under the effect of gravity alone, would settle into the lower stream. Those particles that do settle into the lower stream during the initial transient phase, however, acquire a larger penetration distance [cf. Fig. 12(c)], so that even at time 60 the weighted displacement thickness for Fr=8 is the same as for particles settling into still fluid. Eventually it will, of course, have to fall behind, as the supply of further particles entering into the lower stream is cut off. Even for Fr=5, the mixing layer still reduces the number of particles entering the lower stream, but this effect

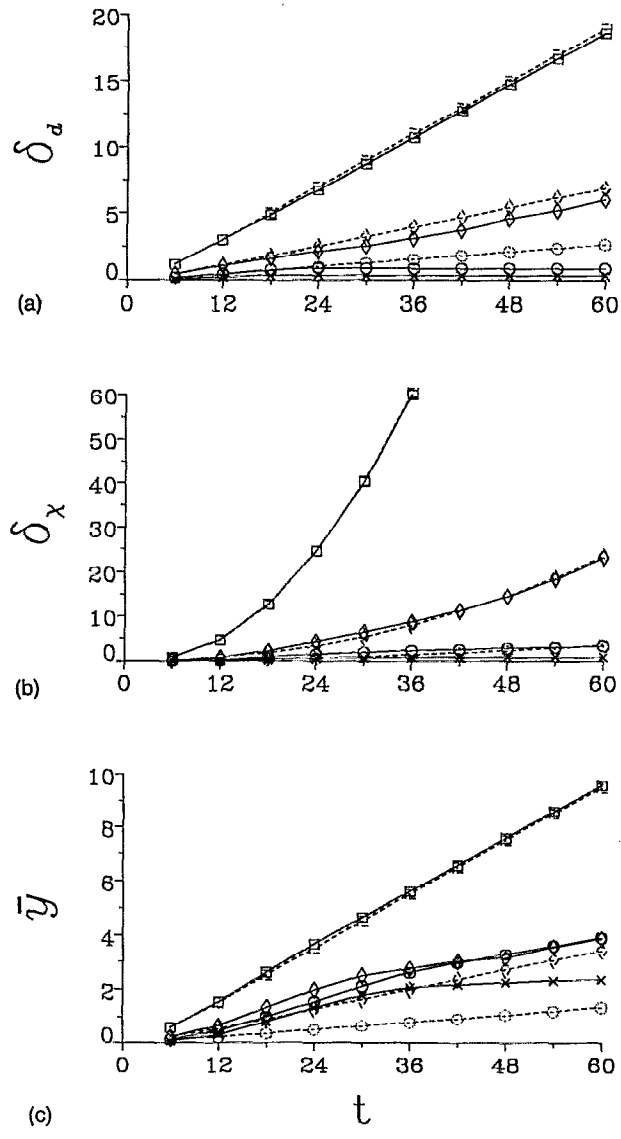

FIG. 12. (a) Displacement thickness, (b) weighted displacement thickness, and (c) average distance of penetration for St=3; ×, Fr=∞; ○, Fr=8; ◇, Fr=5; and □, Fr=3. Solid lines indicate particle settling through the mixing layer, while dashed lines denote particle settling in still fluid. The suspension mode is clearly identifiable for Fr=8, as δ_d remains constant for $t>25$, i.e., no more particles enter the lower stream. Even for stronger gravity, the tendency toward suspension reduces the number of dispersed particles.

decreases monotonically as gravity becomes relatively more important. For Fr=3, all three of the scales shown in Fig. 12 are nearly unaffected by the presence of the mixing layer. The figure furthermore suggests that in the limit as Fr→0, the mixing layer does not affect the quantitative measures of particle dispersion at all. This means that in this limit, the difference in the displacements of a particle falling in still fluid and one falling through the mixing layer vanishes. This displacement difference can be obtained by taking the time integral over the velocity difference between the two particles. In the limit of Fr→0, the mixing layer affects the particle over a shorter and shorter time, meaning that a velocity difference exists over a shorter and shorter time. Consequently, the net displacement between the two particles approaches zero. A more mathematical argument to this end is presented in the Appendix. One has to keep in mind, however, that for very strong gravity the slip velocity between particle and fluid will become quite large, so that a nonlinear drag law should be applied instead of the present Stokes drag law.

The above results lead to an important conclusion: For small values of St, the presence of the mixing layer increases the number of settling particles, whereas for larger values of St it tends to reduce it slightly. The weighted displacement thickness, which for small St also shows an increase due to the presence of the mixing layer, remains largely unaffected by it for larger St. The calculations indicate the existence of three distinct settling regimes: For large values of $\mathrm{St/Fr^2}$, gravity dominates the transport of particles into the lower stream, with a modulation due to the contribution of the coherent vortices. For intermediate values of $\mathrm{St/Fr^2}$, the Kelvin–Helmholtz vortices provide the main mechanism for ejecting particles into the opposite stream. In this regime, the coherent vortices can furthermore create large concentration nonuniformities for particles of intermediate St values. Finally, for small $\mathrm{St/Fr^2}$ complete suspension can occur, so that after an initial transient period the transport of particles from the upper into the lower stream is cut off completely. For the purpose of distinguishing these different settling regimes, it is useful to rescale both time, displacement thickness, weighted displacement thickness, and average distance of penetration,

$$t^*=\frac{t}{\mathrm{St}},\quad \delta_d^*=\delta_d\frac{\mathrm{Fr}^2}{\mathrm{St}^2},\quad \delta_\chi^*=\delta_\chi\frac{\mathrm{Fr}^4}{\mathrm{St}^4},\quad \bar{y}^*=\bar{y}\frac{\mathrm{Fr}^2}{\mathrm{St}^2}. \tag{22}$$

From the above equations, (20) and (21), we then obtain for settling under gravity, in still fluid, the universal relationships,

$$\delta_{dg}^*=e^{-t^*}-1+t^*,\quad \delta_{\chi g}^*=\tfrac{1}{2}(e^{-t^*}-1+t^*)^2,\quad \bar{y}_g^*=\tfrac{1}{2}(e^{-t^*}-1+t^*), \tag{23}$$

which are valid for all values of St and Fr. In Fig. 13, these relationships are shown, along with the results for the four calculations discussed in detail above in Figs. 1–4. The computational results for the two gravity-dominated cases follow the universal relationships quite accurately.

The derivation of a scaling law for the particle transport into the initially void stream in a turbulent mixing layer without gravity is not as straightforward. For single-phase turbulent mixing layers forming from laminar boundary layers, Browand and Latigo[23] were able to measure the growth of the vorticity thickness l with streamwise distance x as a function of the velocity ratio λ,

$$\frac{dl}{dx}=0.170\lambda, \tag{24}$$

where

$$\lambda=\frac{\Delta U}{U_1+U_2}. \tag{25}$$

For a temporally growing turbulent mixing layer in a reference frame moving with $(U_1+U_2)/2$, this results in

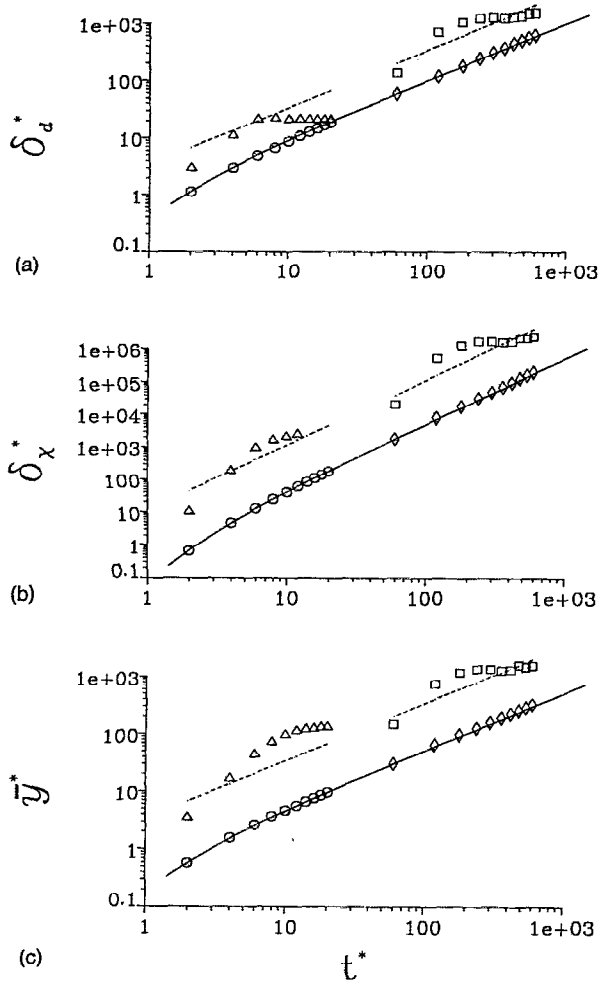

FIG. 13. Rescaled (a) displacement thickness, (b) weighted displacement thickness, and (c) average distance of penetration for the flows described in Figs. 1–4. Comparison between simulation data (disconnected symbols) and scaling laws (lines): ◇, St=0.1, St/Fr^2=0.123; □, St=0.1, St/Fr^2=0.006 25; ○, St=3, St/Fr^2=0.33; and △, St=3, St/Fr^2=0.006 25. The solid lines denote the scaling laws derived for settling in still fluid. The data for settling through the mixing layer in the presence of strong gravity show good quantitative agreement with these scaling laws. The dashed lines describe the scaling laws derived for a turbulent mixing layer with self-similar growth. The permanent suspension observed in the calculation for St=3, St/Fr^2=0.006 25 prevents agreement, as does the lack of additional subharmonic perturbations that could fuel further growth.

$$\frac{dl}{dt}=0.085\ \Delta U. \tag{26}$$

In order to obtain a rough estimate for the number of particles transported from the upper stream to the lower stream through the effect of the coherent vortices, we assume that by time t the mixing layer has entrained all the particles that in the unperturbed flow are located between $y=0$ and $y=l(t)/2$, and redistributed them evenly between $y=-l(t)/2$ and $y=l(t)/2$. This assumption can be expected to hold approximately for small values of St, where particles follow the fluid, and fluid from the upper and lower stream is mixed approximately evenly. For larger St, the accuracy of the assumption obviously is more questionable, since earlier we found that the particle concentration generally is nonuniform in the mixing layer, but it can still serve as a first estimate for comparison purposes. For the displacement thickness, weighted displacement thickness, and average distance of penetration, we then obtain

$$\delta_{d\mathrm{ml}}^*=0.021\,\frac{\mathrm{Fr}^2}{\mathrm{St}}\,t^*,\quad \delta_{\chi\mathrm{ml}}^*=0.000\,44\,\frac{\mathrm{Fr}^4}{\mathrm{St}^2}\,t^{*2},$$
$$\bar{y}_{\mathrm{ml}}^*=0.021\,\frac{\mathrm{Fr}^2}{\mathrm{St}}\,t^*. \tag{27}$$

Lazaro and Lasheras[5] scale their data for particle dispersion in a spatially growing mixing layer in a corresponding fashion. They present data for δ_L/St as a function of x/St. Here δ_L indicates the 0.1–0.9 level thickness, and x denotes the downstream distance measured from the trailing edge of the splitter plate. Their data show collapse for various values of St. Unfortunately, the authors do not present data for a scaled integral thickness of the concentration field. On the other hand, our concentration data at times show several crossings of the 0.1 and 0.9 levels, so that we cannot directly compare with their results. For the two calculations St=3, St/Fr^2=0.006 25 and St=0.1, St/Fr^2=0.006 25, the above relationships are plotted in Fig. 13, along with the results of the corresponding computations. We find that the order of magnitude given by the above relationships (25) is correct, but the agreement is far from accurate. For early times, the disagreement is mostly due to the fact that the growth of the mixing layer is determined by the growth rate of the Kelvin–Helmholtz instability and not yet the Browand–Latigo[23] relationship. At later times, the calculation for St=3, St/Fr^2=0.006 25 leads to suspension and thereby to a complete cutoff of the particle transport into the lower stream. Even the simulation for St=0.1, St/Fr^2=0.006 25 cannot be expected to follow the similarity law accurately, since no subharmonic perturbations are present to fuel the continued growth of the mixing layer according to the Browand–Latigo[23] relationship. Hence, for long times this simulation is expected to approach the similarity laws (21) for the gravity dominated case. An additional point concerns the importance of the initial perturbation amplitude in the numerical simulation. Its value determines how long it takes before the Kelvin–Helmholtz instability first saturates and before vortex pairing can affect the mixing layer growth. In this way, different values for the initial perturbation amplitude can shift the computational results to smaller or larger dimensionless times. Consequently, the comparison between computational results and scaling laws should focus more on the slope of the data than on the values themselves.

The above considerations suggest that the contribution of the coherent vortices to the particle transport into the lower stream will be dominant if

$$\frac{d(l/2)}{dt}>V_s, \tag{28}$$

where V_s denotes the settling velocity. This leads to the relationship

$$\frac{\mathrm{St}}{\mathrm{Fr}^2}\simeq 0.042, \tag{29}$$

for the boundary between the vortex-dominated and the gravity-dominated settling regimes.

The above data clearly show that the integral scales for particle settling through a mixing layer cannot be obtained by merely adding those for settling in still fluid and those for dispersion by a mixing layer, due to the inherent nonlinearity of the problem. Rather, the integral scales have to be interpreted as having contributions from (i) the mixing layer alone, (ii) gravity alone, and (iii) the interaction between the mixing layer and gravity. The displacement thickness, which gives a measure of the number of particles dispersed into the unseeded stream, can thus be expressed as a sum of three contributions:

$$\delta_d = \delta_{d\mathrm{ml}} + \delta_{dg} + \delta_{di}, \tag{30}$$

where the subscript ml stands for mixing layer alone contribution, subscript g for the contribution from settling under gravity alone, and subscript i indicates the contribution from the interaction effect. Similarly, the average distance of penetration can be rewritten as

$$\bar{y} = \bar{y}_{\mathrm{ml}} + \bar{y}_g + \bar{y}_i. \tag{31}$$

The weighted displacement thickness is the product of the displacement thickness and the average distance of penetration, i.e.,

$$\delta_\chi = \delta_d \cdot \bar{y}, \tag{32}$$

and it can be rewritten as

$$\delta_\chi = \delta_{d\mathrm{ml}} \cdot \bar{y}_{\mathrm{ml}} + \delta_{dg} \cdot \bar{y}_g + \delta_{d\mathrm{ml}} \cdot \bar{y}_g + \delta_{dg} \cdot \bar{y}_{\mathrm{ml}} + \bar{y}_i \cdot (\delta_{d\mathrm{ml}} + \delta_{dg}) + \delta_{di} \cdot (\bar{y}_{\mathrm{ml}} + \bar{y}_g + \bar{y}_i). \tag{33}$$

From the above equation it is clear that in the absence of any interaction effect (i.e., $\delta_{di} = 0$ and $\bar{y}_i = 0$), the mixing layer and gravity contribute the first four terms on the right-hand side. Hence, it can be deduced that the interaction effect on the weighted displacement thickness is

$$\delta_{\chi i} = \delta_\chi - \delta_{d\mathrm{ml}} \cdot \bar{y}_{\mathrm{ml}} - \delta_{dg} \cdot \bar{y}_g - \delta_{d\mathrm{ml}} \cdot \bar{y}_g - \delta_{dg} \cdot \bar{y}_{\mathrm{ml}}. \tag{34}$$

Figures 14 and 15 show the interaction effect for two Stokes numbers (St=0.1 and 3.0) and various Froude numbers. The general trend is that it is negative for all three measures of the settling process, for all values of St and Fr. Furthermore, the magnitude of the interaction effect increases with decreasing Fr. In other words, even though we observed enhanced settling of particles with St=0.1 and St/Fr^2=0.123 as a result of the presence of the mixing layer, the dispersion measures are still lower than the sum of the separate mixing layer and gravity effects. The figures show that generally for early times, the magnitude of the interaction effect increases with growing importance of gravity. A strong initial growth of both number and distance is typically followed by a leveling off at later times. However, for those cases with weak gravity that tend to generate particle suspension, the magnitude of the interaction effect for the displacement thickness can grow to levels larger than for strong gravity.

Part 1 of this investigation (mm) had confirmed earlier findings of optimal dispersion in the absence of gravity for particles characterized by St values near unity. In particular, we had found that only the weighted displacement thickness

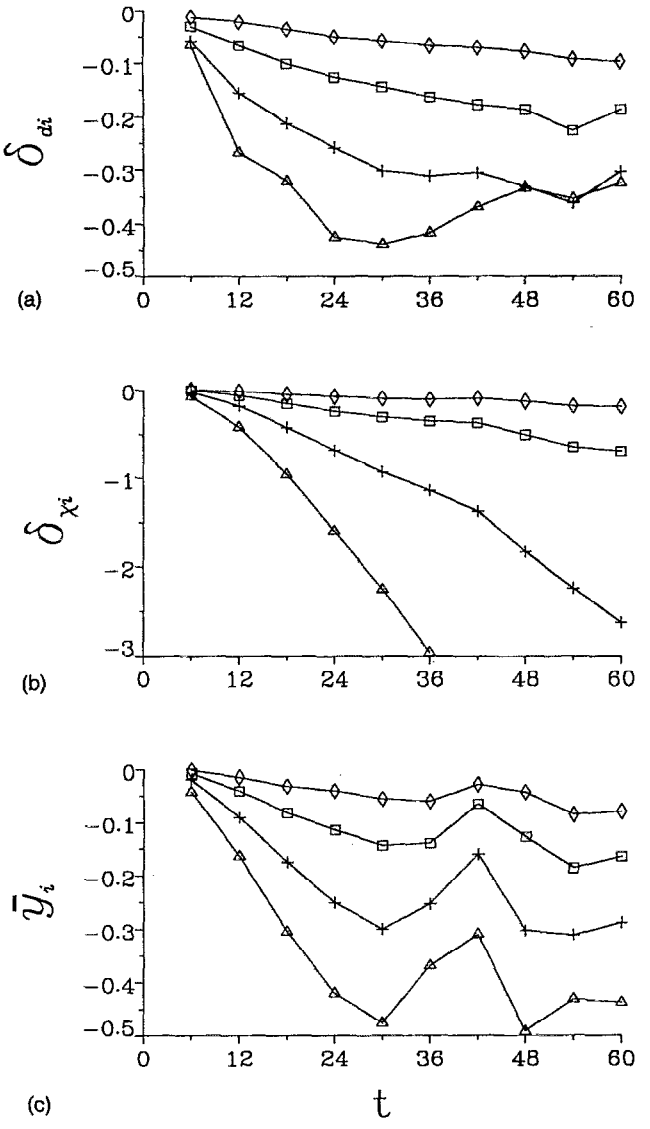

FIG. 14. The interaction effect on (a) displacement thickness, (b) weighted displacement thickness, and (c) average distance of penetration for St=0.1; ◇, Fr=5; □, Fr=3; +, Fr=2; and △, Fr=1.5. The interaction effect is negative and increases in magnitude with increasing importance of gravity. This indicates that the particle transport for settling through a mixing layer is smaller than the sum of the particle transport achieved by the mixing layer alone and the transport due to settling in still fluid.

shows a maximum for intermediate values of St, whereas the number of dispersed particles decreases monotonically with increasing St. In order to see if this optimal dispersion persists in the presence of gravity, we conducted a series of simulations in which the value of St was varied, while the terminal settling velocity was held constant. Figure 16 shows that, after some time, both the number of particles and the weighted displacement thickness show a maximum for intermediate values of St. However, in contrast to the simulations without gravity, the optimal value of St decreases with time, to values near 0.5.

2. Influence of particle Reynolds number

So far we have assumed that the drag on the particle is given by the Stokes drag law, which is valid for small par-

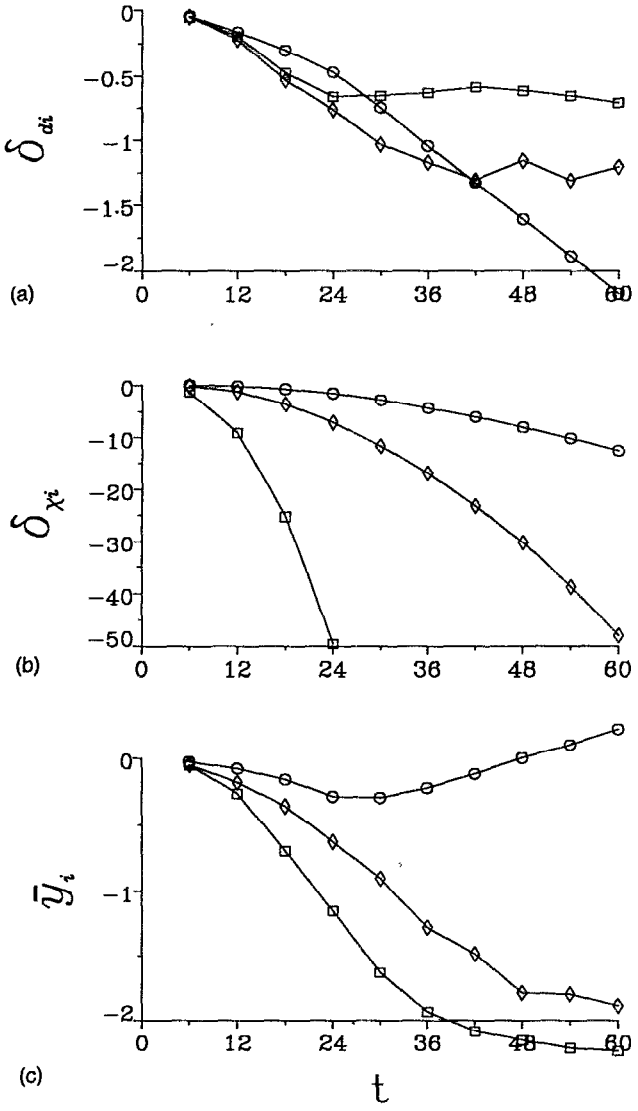

FIG. 15. The interaction effect on (a) displacement thickness, (b) weighted displacement thickness, and (c) average distance of penetration for St=3; ○, Fr=8; ◇, Fr=5; and □, Fr=3. For short times, the magnitude of the interaction effect increases with gravity. For longer times, however, the nearly steady-state velocity field results in the suspension of the lighter particles, thereby cutting of their transport into the unseeded stream, which increases the size of the interaction effect (δ_{d_i}) for weak gravity.

ticle Reynolds numbers only. At higher particle Reynolds numbers, the drag coefficient is higher than that predicted by the Stokes drag law. It is hence of interest to study how the above results are modified at higher particle Reynolds numbers. To this end, we employ the following modified equations:

$$\frac{du_p}{dt}=\frac{f}{\mathrm{St}}(u-u_p),$$

$$\frac{dv_p}{dt}=\frac{f}{\mathrm{St}}(v-v_p)-\frac{1}{\mathrm{Fr}^2},$$

where f is given by the following empirical relation (Clift *et al.*[24]):

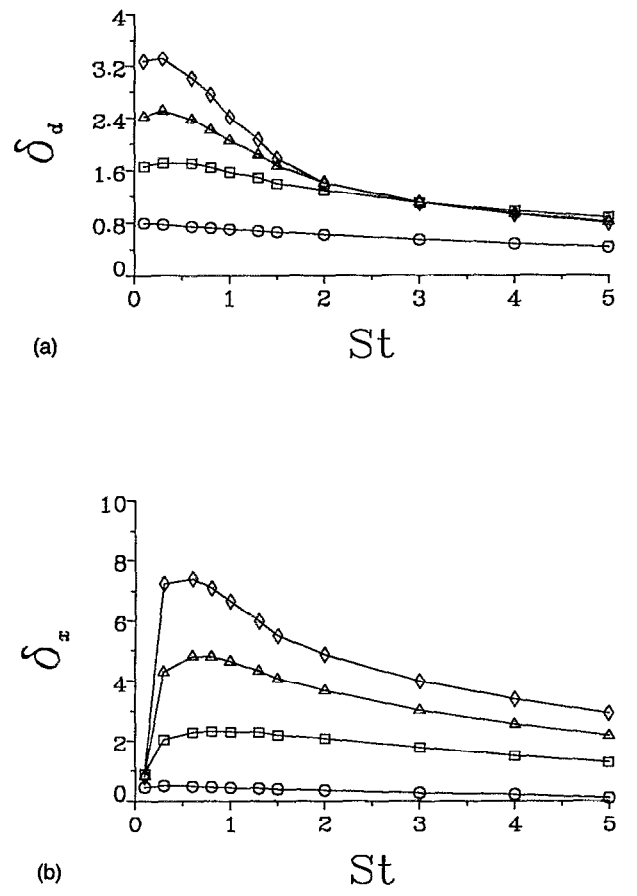

FIG. 16. (a) Displacement thickness and (b) weighted displacement thickness for St/Fr^2=0.06 25 as a function of St; ○, $t=12$; □, $t=24$; △, $t=36$; and ◇, $t=48$. For constant terminal velocity, the dispersion is maximized for intermediate values of St. The optimal value for St is slightly less than 1, and it tends to decrease with increasing time.

$$f=1+0.15\ \mathrm{Re}_p^{2/3},\quad \mathrm{Re}_p=\frac{|\mathbf{u}-\mathbf{v_p}|d_p\,\Delta U}{\nu}.$$

Here $|\mathbf{u}-\mathbf{v_p}|$ is the magnitude of the dimensionless slip velocity of the particle. The above drag law has been employed in the past by, among others, Chein and Chung.[3] If we denote the quantity $d_p\,\Delta U/\nu$ by $\mathscr{R}$, then there are now three parameters: St, Fr, and $\mathscr{R}$ in the governing equations. We study the case in which St=3, Fr = $\sqrt{480}$, and $\mathscr{R}$=100 (Fig. 17), which typically leads to maximum particle Reynolds numbers of $O(30)$ in the vortical region of the flow field. Comparison with Fig. 3(d), which shows the same case for Stokes' drag law, indicates that in the present case the accumulation of particles in the braid region is more pronounced. In this sense, particles with St=3 and a larger particle Reynolds number behave similarly to particles with lower values of St and particle Reynolds number, as long as f/St remains comparable.

In addition, the increased drag at higher particle Reynolds numbers reduces the settling velocity, so that again particles with larger values of St and Reynolds number behave similar to those with lower values for both of these parameters. Thus, the present simulation suggests that the dispersion trends of particles at higher Reynolds numbers are

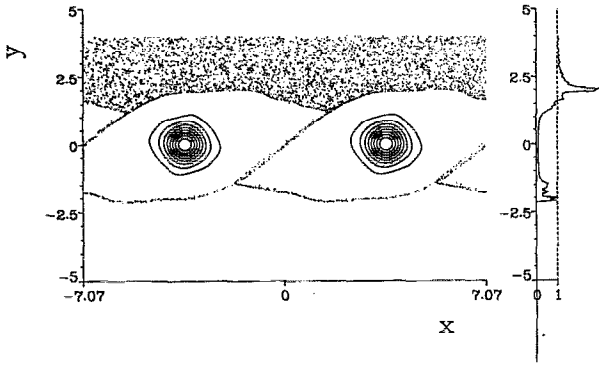

FIG. 17. Particle positions and concentration for St=3.0, St/Fr^2=0.006 25 and $\mathscr{R}$=100 at t=30. Increasing the Reynolds number increases the accumulation in the braid region apart from decreasing the average distance of penetration [compare with Fig. 3(d)].

qualitatively similar to those at lower Reynolds numbers, provided the Stokes number is reduced correspondingly. Having investigated how increasing the particle Reynolds number modifies the dispersion characteristics, we return to the low Reynolds number situation in the following sections.

3. Effect of subharmonic perturbation

Repeated vortex pairing is known to be the dominant growth mechanism in mixing layers (Winant and Browand[25]). It involves an ongoing reorganization of the mixing layer vorticity, and thereby maintains a continuously evolving fluid velocity field. Since the distribution of the particles in the flow depends on the time integral over the fluid velocities, we have to expect the dynamics of the pairing process to play a crucial role for the time-dependent development of the particle concentration field. This was confirmed by the simulations of mixing layers without gravity by Chein and Chung[3] and MM, as well as by the experiments of Kiger and Lasheras,[26] in which the effect of gravity was small as well. In the following, we will investigate the effects of one pairing event on the settling process of the particles through the mixing layer. It should then be possible to model the role of subsequent pairing events by appropriately rescaling the relevant quantities. In order to trigger vortex pairing in the numerical simulation, we double the length of the control volume and perturb the initial vorticity distribution by a subharmonic wave in addition to the basic disturbance. The phase of the subharmonic is chosen such that it reaches a maximum midway between the two evolving vortices. In this way, the two equally strong vortices will proceed toward a pairing event rather than a tearing process. In order to elucidate the effect of vortex pairing on the dispersion and settling process, we will focus on the same parameter combinations for which we presented detailed results above.

Figure 18 shows the evolution of both the vorticity field and the particle concentration field for St=0.1 and St/Fr^2=0.006 25. By time t=24, the vortices are well on their way toward a pairing event, and the effect of their motion on the particle field is clearly visible. As for the case of a basic perturbation only, the strands of clear and particle-

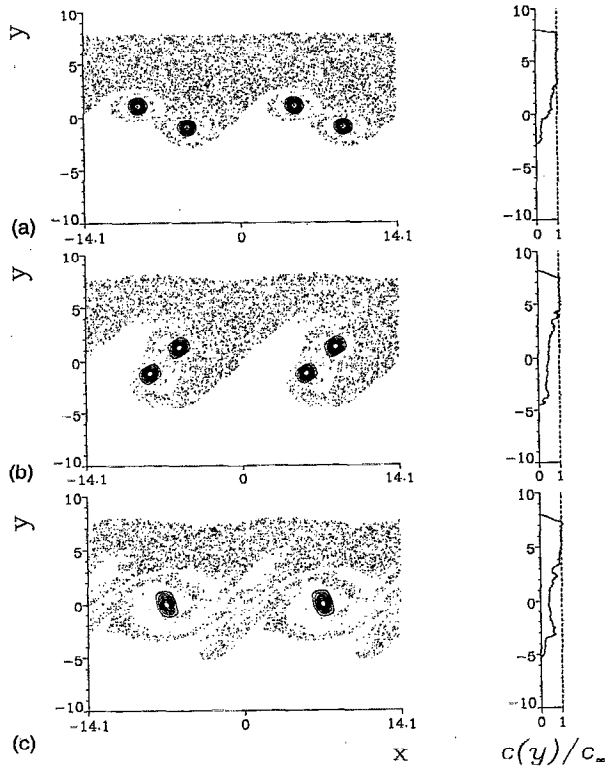

FIG. 18. Mixing layer with basic and subharmonic perturbation. Particle positions and concentration for St=0.1, St/Fr^2=0.006 25. (a) t=24; (b) t=36; and (c) t=60. The particles have only a small slip velocity, so that the near point symmetry of the clear fluid and the particle-laden fluid is maintained. The unsteady vortex motion leads to a strong mingling and filamentation of the clear and particle-laden fluid regions. Compared to the case without a subharmonic perturbation, a larger part of the flow field is swept out by the vortices, which enhances the particle transport into the unseeded stream.

laden fluid develop in a nearly point-symmetric fashion with respect to both the centers of the evolving pairs and the midpoint between vortex pairs. However, as a result of the unsteady vortex motion, a much larger section of the seeded stream is now affected by the vortices, so that the plateau-like region of the $c(y)/c_\infty$ distribution extends over a larger domain at t=36. Furthermore, the continued motion of the coherent vortices around each other leads to a more intense stretching, deformation, and filamentation of the clear and particle-laden fluid strands; cf. the investigation by Meiburg *et al.*[27] for passive fluid particles. As a result, by the end of the pairing process around t=60, we observe very distorted regions of particle-laden fluid intermingled with regions void of particles, so that the overall particle distribution is more homogeneous than for the case of a fundamental perturbation only. This is in agreement with the experimental findings of Kiger and Lasheras.[26]

For St=0.1 and St/Fr^2=0.123, the effect of the subharmonic perturbation is relatively minor. As for the case of a basic perturbation only, each vortex creates a relatively small region of lower particle concentration amid the rapidly settling particles. As the vortices pair, these void regions merge to form a slightly bigger one. Overall, the concentration distribution $c(y)/c_\infty$ again shows a dip in the mixing layer re-

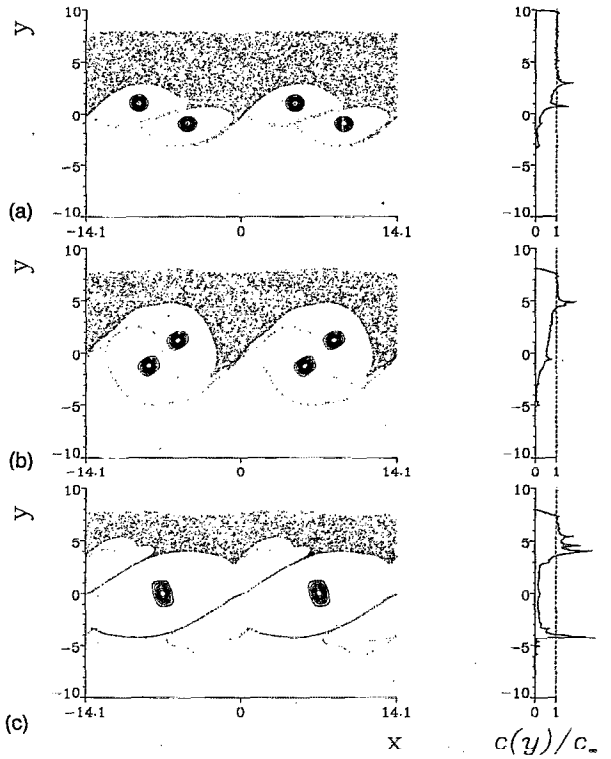

FIG. 19. Mixing layer with basic and subharmonic perturbation. Particle positions and concentration for St=3, St/Fr^2=0.006 25. (a) $t=24$; (b) $t=36$; and (c) $t=60$. The intense strain between pairing vortices depletes this region of particles, so that the void regions around the individual vortices merge. The inertia of the particles leads to a complex shape of the void regions in unsteady flow, and it allows for the convection of void regions away from the vortices.

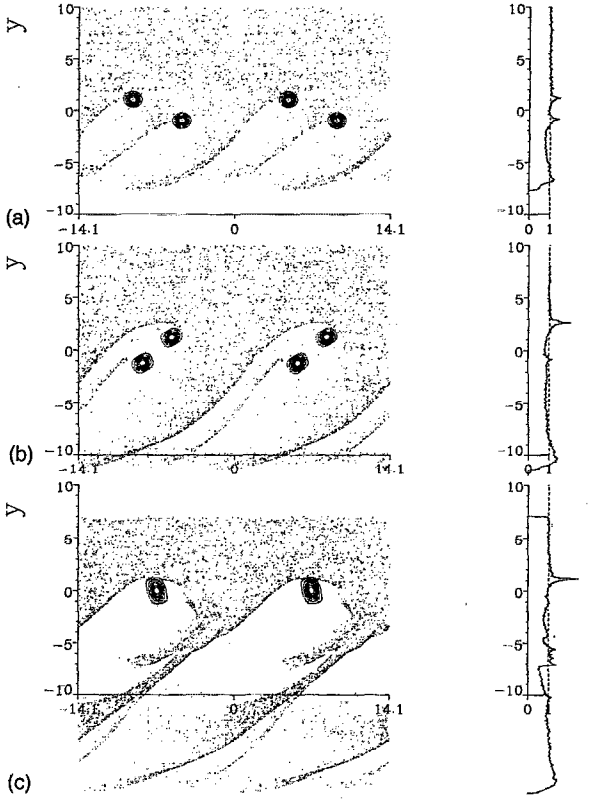

FIG. 20. Mixing layer with basic and subharmonic perturbation. Particle positions and concentration for St=3, St/Fr^2=0.33. (a) $t=24$; (b) $t=36$; and (c) $t=60$. Particle bands emerge from regions near the vortex cores. The vortex pairing process leads to a merging of the particle bands as well.

gion, indicating that the coherent vortices speed up the settling process.

For heavier particles, the situation changes fundamentally. Figure 19 indicates that for St=3 and St/Fr^2=0.006 25 large void regions quickly form around the vortex centers, separated by concentrated bands of heavy particles. In between pairing vortices the strain field is considerably more intense than in between vortex pairs, so that particles are ejected from this region, thereby allowing the void regions around the individual vortices to merge by $t=36$, similarly to the scenario described by MM for the case without gravity. In the following, the void regions around the vortex pairs undergo a strong deformation, partially due to the instantaneous evolution of the fluid velocity field and partially as a result of the time-integrated effect of the fluid velocities on the particles, which for these larger values of St is more important. The resulting complex shapes of these void regions lead to the evolution of several sharp spikes in the $c(y)/c_\infty$ profile by $t=60$, both above and below the mixing layer. Due to the time integration effect, hence it seems possible that such void regions can be convected away from vortex cores and survive in irrotational flow regions for time intervals up to $O(\mathrm{St})$. Furthermore, it is obvious that the continued unsteadiness of the flow field renders suspension of the particles more unlikely. This suspension relies on the particles' bouncing off the vortices in a very regular manner; cf. Gañan-Calvo and Lasheras,[13] which is most easily achieved in steady flows. Hence, we can conclude that the continued unsteadiness due to repeated vortex pairing renders the suspension mode less important.

For St=3 and St/Fr^2=0.333, during the early stages we again observe the formation of bands that emanate from near the vortices and reach into the lower, initially unseeded stream; cf. Fig. 20(a). However, as these vortices proceed toward a pairing event, they will move through the band of their pairing partner, Figs. 20(b), and 20(c), thereby effectively disrupting the connection between the band and its former vortex. The result is a partial merger of the bands of the two pairing vortices, similar to the observation by Kiger and Lasheras[26] for the case with negligible gravity, so that the distance between neighboring bands effectively doubles. However, for these larger values of St time integration effects remain important, so that the bands show some filamentation and do not become as sharply focused as for the case of a basic perturbation only.

The above mechanisms are again reflected by the quantitative data for the RMS values of the particle concentration fields at $t=30$ (Fig. 21). For St=0.1, the particles again follow the fluid, so that the concentration levels are either zero or unity. Consequently, the RMS values are near one-half. For St=3, on the other hand, we observe RMS values in excess of 2, indicating the ability of the vortical structures to

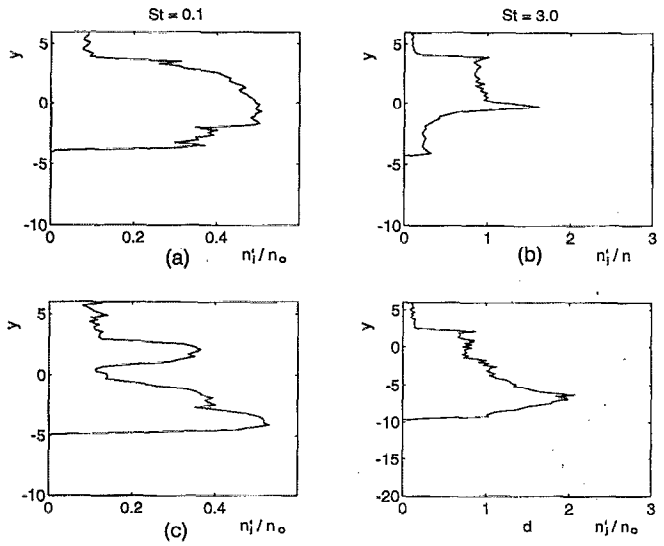

FIG. 21. Mixing layer with basic and subharmonic perturbation. Root mean square of the particle concentration field along lines y=const. at t=30; (a) St=0.1, St/Fr^2=0.006 25; (b) St=3, St/Fr^2=0.006 25; (c) St=0.1, St/Fr^2=0.123; and (d) St=3, St/Fr^2=0.33. As for the basic perturbation case, the RMS values for St=0.1 do not exceed $\frac{1}{2}$. The decreased importance of the suspension mode in the presence of vortex pairing leads to a broader peak in frame (b).

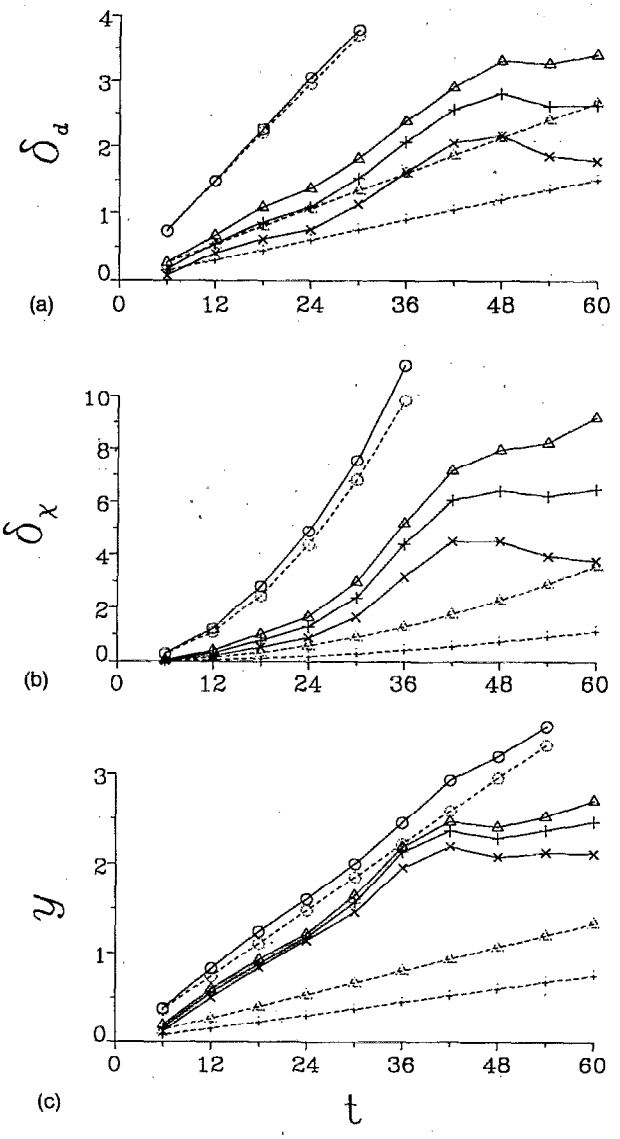

FIG. 22. Mixing layer with basic and subharmonic perturbation. (a) Displacement thickness, (b) weighted displacement thickness, and (c) average distance of penetration for St=0.1; ×, Fr=∞; +, Fr=2; △, Fr=1.5; and ○, Fr=0.9. Solid lines indicate the case of particle settling through a mixing layer, while dashed lines denote settling in still fluid. The presence of the mixing layer consistently leads to increased particle transport. All three dispersion measures are enhanced by the subharmonic perturbation, and they grow with increasing importance of gravity.

create strong concentration nonuniformities, in the shape of suspension or bands.

The results for the displacement thickness, the weighted displacement thickness, and for the average penetration distance are also similar to the ones seen earlier for the case of a basic perturbation only. For small values of St, the mixing layer leads to an increase in the number of settling particles (Fig. 22), while for larger St this number is slightly reduced (Fig. 23). Both weighted displacement thickness and average penetration distance are consistently enhanced by the presence of the mixing layer. In addition, the effect of the mixing layer in dispersing the particles is more prominent here than in the basic perturbation case, for all values of the Froude number. This enhanced dispersion is caused by the increased unsteadiness in the flow field. In particular, the data for St=3 and Fr=8 confirm the reduced importance of the suspension mode in the presence of vortex pairing. While in the absence of pairing the particle transport was effectively cut off once the basic disturbance had saturated, particle settling continues in the presence of the subharmonic until the paired vortices reach a nearly steady state. It is reasonable to assume that in the presence of further subharmonic disturbances particle settling will continue indefinitely.

The comparison with the similarity laws derived earlier reflects the influence of the pairing as well (Fig. 24). For the two cases of larger terminal velocities, the data again agree well with the similarity laws for flows dominated by gravity. For the cases where dispersion is dominated by the coherent vortices, we get good agreement between the slope of the data and that of the similarity laws, once the initial transient has passed, during which the flow is dominated by the Kelvin–Helmholtz instability growth rather than by pairing processes. As discussed earlier, a change in the initial perturbation amplitude would shift the computational data in the horizontal direction, so that this slope represents the only meaningful quantity comparison. In particular, the graphs reflect the breakup of the beginning suspension mode due to the growth of the subharmonic disturbance.

C. Vertical flow

If the mean flow is either aligned with or opposite to the direction of the gravitational acceleration, gravity cannot directly affect the cross-stream particle velocity component and the quantitative dispersion measures. It can do so only indirectly by modifying the streamwise particle velocity. The set of governing equations now is

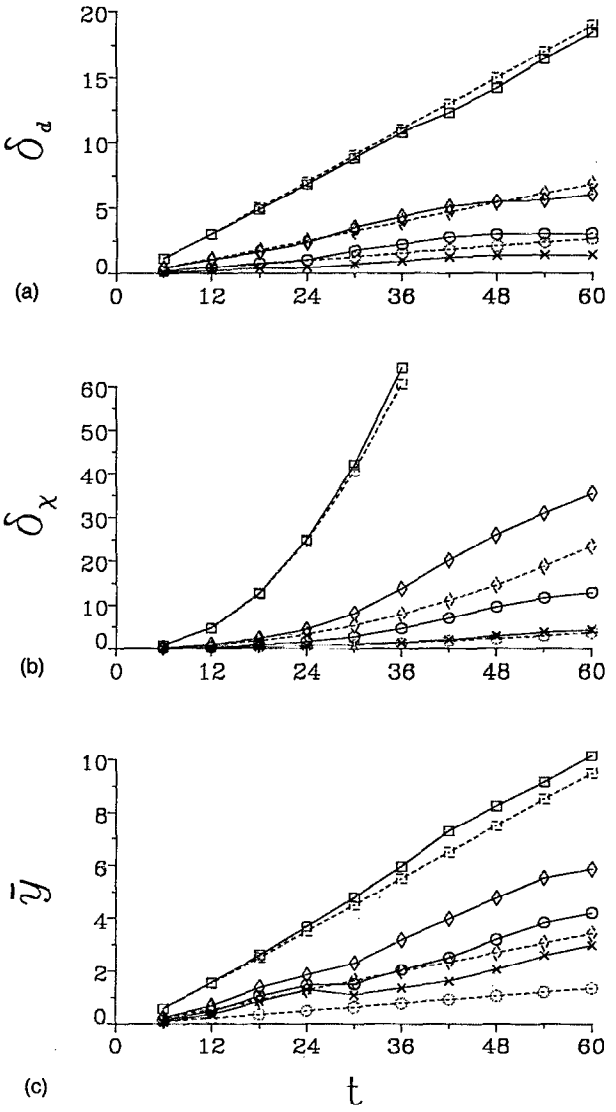

FIG. 23. Mixing layer with basic and subharmonic perturbation. (a) Displacement thickness, (b) weighted displacement thickness, and (c) average distance of penetration for St=3; ×, Fr=∞; ○, Fr=8; ◇, Fr=5; and □, Fr=3. Solid lines indicate the case of particle settling through a mixing layer, while dashed lines denote settling in still fluid. The subharmonic perturbation decreases the tendency of the particles to become suspended. Notice that, in particular, for Fr=8, particle settling now continues throughout the pairing process, until the fluid velocity field reaches a nearly steady state. This indicates that flow unsteadiness counteracts the tendency toward particle suspension.

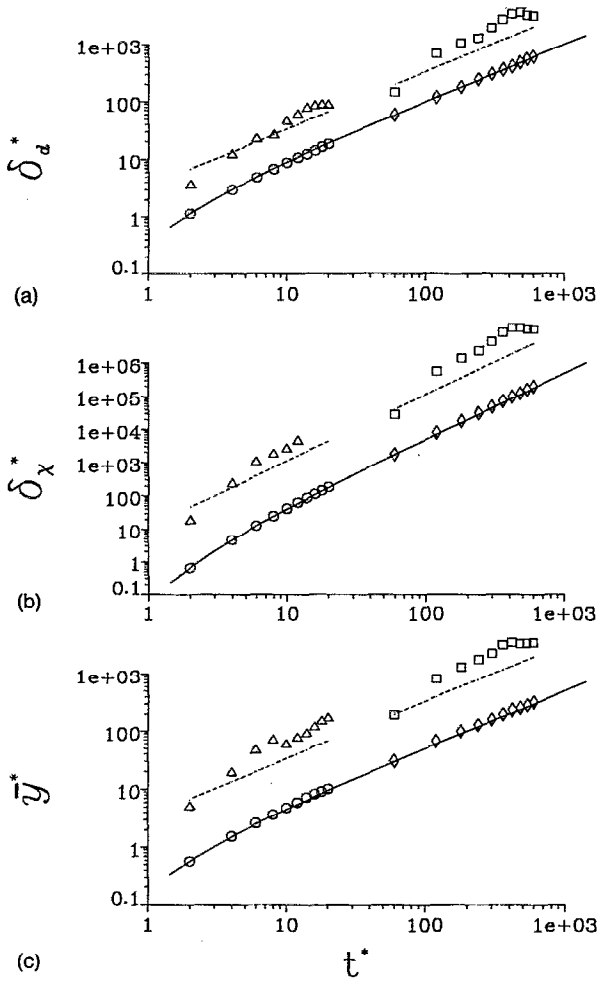

FIG. 24. Mixing layer with basic and subharmonic perturbation. Rescaled (a) displacement thickness, (b) weighted displacement thickness, and (c) average distance of penetration. Comparison between simulation data (disconnected symbols) and scaling laws (lines): ◇, St=0.1, St/Fr^2=0.123; □, St=0.1, St/Fr^2=0.006 25; ○, St=3, St/Fr^2=0.33; and △, St=3, St/Fr^2=0.006 25. The data for settling through the mixing layer in the presence of strong gravity again show good quantitative agreement with scaling laws derived for settling in still fluid (solid lines). The dashed lines describe the scaling laws derived for a turbulent mixing layer with self-similar growth. Up to the time at which further growth of the mixing layer is prevented by the absence of additional subharmonic disturbances, the slope of the data agrees reasonably well with that of the scaling laws.

$$\frac{du_p}{dt}=\frac{1}{\mathrm{St}}(u-u_p)\pm\frac{1}{\mathrm{Fr}^2}, \tag{35}$$

$$\frac{dx_p}{dt}=u_p, \tag{36}$$

$$\frac{dv_p}{dt}=\frac{1}{\mathrm{St}}(v-v_p), \tag{37}$$

$$\frac{dy_p}{dt}=v_p. \tag{38}$$

The "+" sign holds if the mean flow points in the direction of gravity, i.e., for downward flow, whereas the "−" sign applies to upward flows. Keeping in mind that either the faster or the slower of the two streams can be the seeded one, we then have to distinguish four different situations. However, if we again adopt a reference frame that moves with the average of the two free-stream velocities, the number of different situations is reduced to two: seeding the slower stream in an upward flow corresponds to seeding the faster stream in a downward flow; and seeding the faster stream in an upward flow is equivalent to seeding the slower stream in a downward flow. In other words, we only have to distinguish between the two situations in which the relative velocity of the seeded stream is aligned with or opposite to the direction of gravity.

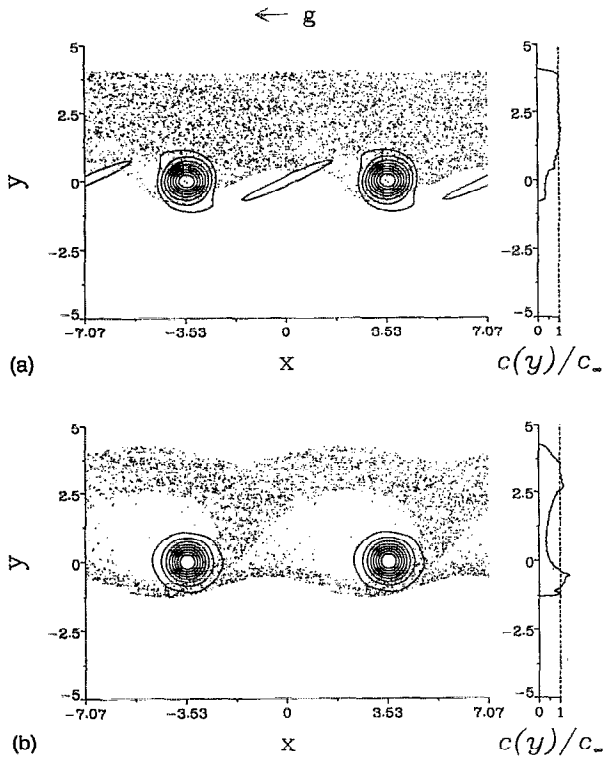

FIG. 25. Upward flow with the faster stream being the seeded one. Particle positions and concentration for St=1 and Fr=1.5, (a) $t=12$; (b) $t=24$. In the reference frame moving with the coherent vortices, the particles have only a small streamwise velocity, which gives the cross-stream fluid velocity component sufficient time to transport the particles across the mixing layer.

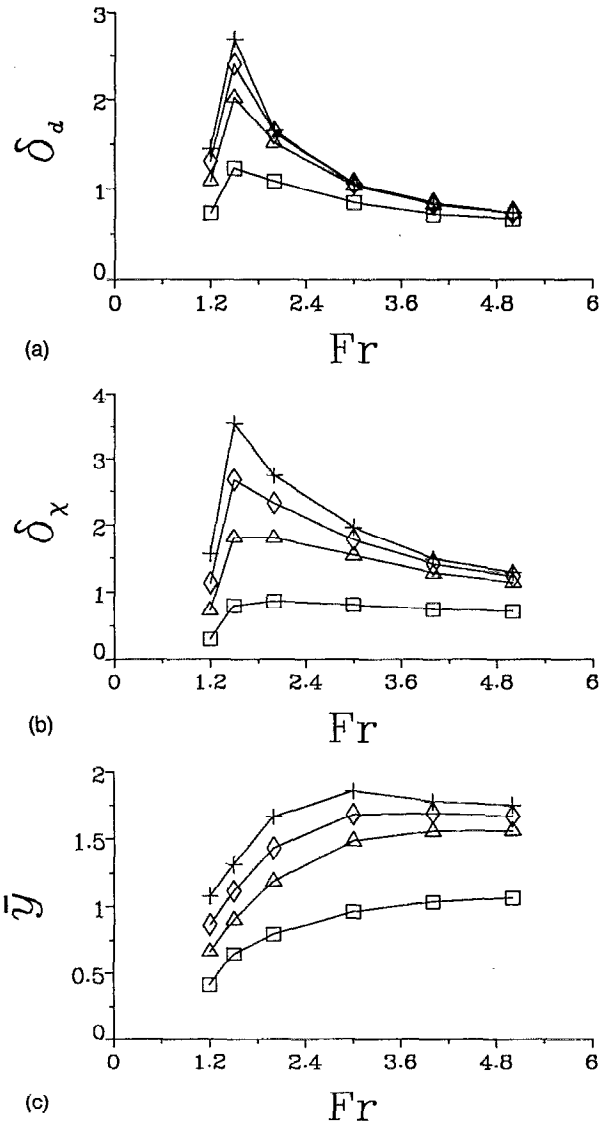

FIG. 26. Upward flow with the faster stream being the seeded one. (a) Displacement thickness, (b) weighted displacement thickness, and (c) average distance of penetration for St=1. □, $t=24$; △, $t=36$; ◇, $t=48$; and +, $t=60$. Dispersion is optimized when the terminal settling velocity of the particles St/Fr^2 equals one-half the difference of the free-stream velocities, so that the particle motion is slow along the streamwise direction in the reference frame moving with the vortices.

We begin by discussing upward flow in which the faster stream is seeded, corresponding to the "−" sign in front of the gravitational term in the above equations. For the relatively small value of St=0.1 and moderate to large values of Fr, the qualitative and quantitative evolution of the particle concentration field is very similar to the case described in Fig. 1. In other words, a flow with a small settling velocity opposite to the direction of the mean flow develops similarly to a flow with a small settling velocity in the cross-stream direction. For the vertical flow, there is, of course, no mechanism comparable to the suspension observed in horizontal flow, since there is no force present that brings particles ejected by the vortices back toward the mixing layer.

For St=1 and Fr=1.5, we encounter a very different situation. Now the settling velocity is nearly equal and opposite to half the difference velocity between the two free streams. Consequently, the particles in the seeded stream move with approximately the same streamwise velocity as the vortices, so that in our moving reference frame they nearly stand still. In this way, the residence time of a particle near a vortex increases, which gives the cross-stream fluid velocity component induced by the vortices more time to affect the particle, thereby increasing its importance. In the upstream half of the braid region, where the cross-stream fluid velocity component points away from the seeded stream, the particles become entrained into the mixing layer [Fig. 25(a), $t=12$]. However, there they encounter smaller streamwise velocities, so that they begin to fall toward the upstream vortex. As they approach this vortex, it ejects them into the initially unseeded stream [Fig. 25(b), $t=24$].

The above qualitative description suggests that the vanishing streamwise relative velocity between the particles in the seeded free stream and the mixing layer vortices represents a crucial prerequisite for the dispersion mechanism to be effective. Only under these conditions can the regions of cross-stream fluid velocities affect the particles long enough to entrain them into the mixing layer. As long as there is a sizable streamwise slip velocity between particles and vortices, the particles will periodically encounter cross-stream fluid velocities of alternating signs, and thereby experience little net entrainment. This is confirmed by the quantitative measures of the dispersion process (Fig. 26). For a constant value of St, both the number of particles as well as the

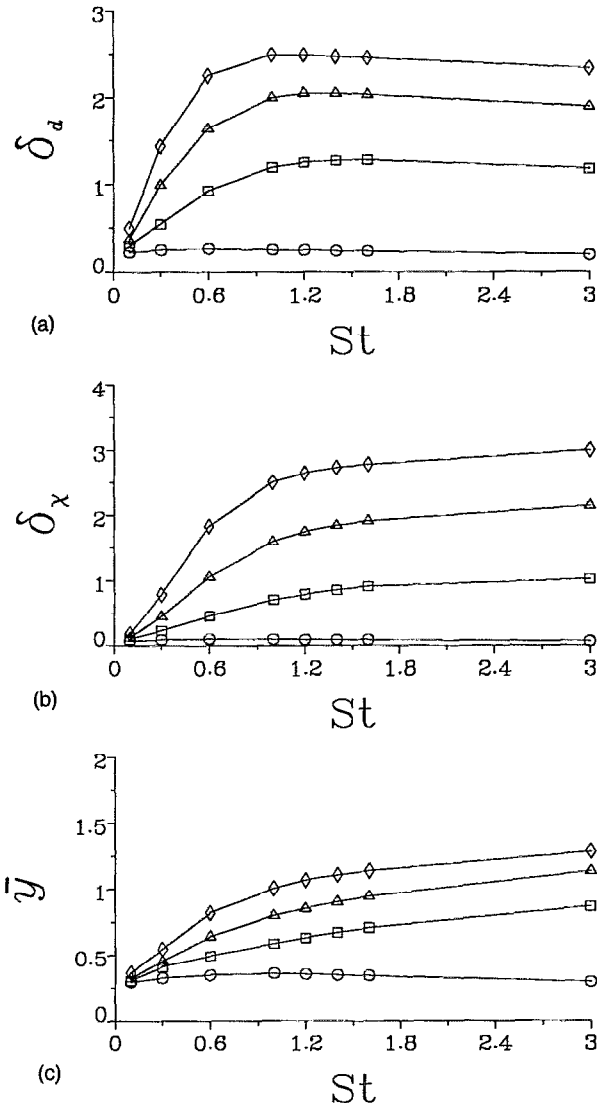

FIG. 27. Upward flow with the faster stream being the seeded one. (a) Displacement thickness, (b) weighted displacement thickness, and (c) average distance of penetration for $St/Fr^2=0.5$. ○, $t=12$; □, $t=24$; △, $t=36$; and ◇, $t=48$. For $St\sim1$, the number of dispersed particles shows a global optimum, whereas both weighted displacement thickness and the distance of penetration do not exhibit an optimum. For $St>1$, these quantities do not strongly depend on St.

weighted displacement thickness exhibit a maximum when $St/Fr^2\approx0.5$, i.e., when the settling velocity is about one-half the difference between the free-stream velocities. This was confirmed for other values of St as well. Only the average penetration distance does not show a maximum. The reason for this can be found in the relative motion of the particles in the initially unseeded stream with respect to the vortices. The relative streamwise velocity between particles and vortices increases monotonically with gravity, thereby rendering the cross-stream velocity component less and less influential. As a result, the average penetration distance decreases with increasing gravity.

By keeping the value of St/Fr^2 at one-half and varying St, we can study the Stokes number effect on the dispersion. For the number of dispersed particles, Fig. 27 shows a slight, but not very pronounced maximum, initially for $St\approx1.5$, later for slightly smaller values. This indicates that even for vertical flows, the dispersion mechanism reaches optimum efficiency when the particle relaxation time approximately equals the characteristic flow time. However, both the weighted displacement thickness and the average distance of penetration do not show such a peak.

A series of simulations in which the relative velocity of the seeded stream was aligned with the direction of gravity did not reveal any interesting new physical mechanisms. Even though we employed a wide variety of $St,St/Fr^2$ combinations, the particle transport into the unseeded stream was always very minimal. The reason for this lies in the large streamwise velocity difference between the particles and the coherent vortical structures. As a result, the particles encounter rapidly changing cross-stream fluid velocity components of alternating sign, so that they never undergo a significant acceleration toward the unseeded stream.

IV. DISCUSSION AND CONCLUSION

The above computational results and theoretical considerations are intended to provide a qualitative and quantitative understanding of the mechanisms that govern the dispersion and settling processes of a dilute particle field in the presence of a mixing layer. For horizontal flow, the two questions "How is the settling under gravity modified by the presence of the mixing layer?," and "How is the particle dispersion by the coherent vortical structures affected by gravity?" represent flip sides of the same coin, and their answers are intimately linked to the mechanisms by which strong nonuniformities can appear in the particle concentration field.

By causing a uniform acceleration of all particles, gravity can introduce concentration inhomogeneities only through its interaction with the vortex-induced particle motion. There are two principally different ways for these inhomogeneties to be created and amplified. First, existing isolines of the particle concentration field can be deformed, stretched, and folded by the fluid velocity field. While this mechanism, in principle, applies to all combinations of St and St/Fr^2, it often dominates for small values of St, where the slip velocity between particles and fluid is small. The result can be a complex filamentation of the particle field, which leads to the intermingling of clear and particle-laden fluid regions, as observed for $St=0.1$ and $St/Fr^2=0.006\,25$. For these low slip velocities, similarities exist with the chaotic transport of passive particles in subharmonically developing mixing layers; cf. Meiburg *et al.*[27] Second, the fluid velocities can cause compressibility effects in the particle velocity field (also cf. MM), thereby leading to depletion of particles in some regions, and to their accumulation in others. For this mechanism to be effective, the particles need to be able to acquire a significant slip velocity, i.e., the value of St cannot be too small. An exception is the suspension mechanism identified by Gañan-Calvo and Lasheras.[13] For a steady flow field, it can be effective over long times and thereby lead to strong particle accumulations in a narrow concentration boundary layer above the vortices, even for small relative velocities, i.e., small St. Under most circumstances, however, repeated vortex pairing will prevent the

formation of a saturated and nearly steady-state flow field, so that the suspension mode decreases in importance.

The second one of the above-mentioned mechanisms represents the way in which vortical structures typically cause concentration nonuniformities: They create a positive divergence in the particle velocity field by ejecting them from their centers. A linear analysis demonstrates that this ejection proceeds with optimal efficiency for intermediate values of St$\sim O(1)$. Near free stagnation points, negative divergence then leads to the accumulation of particles. Again, linear theory shows that this accumulation mechanism works most efficiently for St$\sim$1, even in the presence of gravity.

The above two mechanisms for the creation of an inhomogeneous particle concentration field result in different rms characteristics. The distortion of previously existing isocontours of the particle concentration for small St leads to a concentration field in which the concentration is either near zero or near unity, so that the RMS value of the concentration field cannot exceed one-half. For intermediate values of St, however, the compressibility effect was shown to result in RMS values in excess of 2. To achieve such strong nonuniformities, the mixing layer must be able to affect the particles for sufficiently long times, so that St/Fr^2 cannot be too large.

In order to quantify the combined dispersion and settling process, we focus on the evolution of both the number of dispersed particles and their displacement thickness, as well as on the average distance by which they penetrate the unseeded stream. We find that the number of settling particles is enhanced for small values of St, whereas it is slightly reduced for larger values. The weighted displacement thickness is increased considerably for small St, whereas it remains nearly unchanged for larger St. These findings demonstrate that the effect of the large-scale mixing layer vortices on particle settling is different from that of homogeneous turbulence, for which Wang and Maxey[11] had observed enhanced settling for all values of St. For gravity dominated flow, we find excellent agreement between the computational data and scaling laws derived for settling in still fluid, which indicates that in the limit of strong gravity the influence of the coherent vorticity approaches zero. For weaker gravity, when the dispersion is dominated by the vortical structures, we derive scaling laws based on data for the self-similar growth of turbulent mixing layers according to Browand and Latigo.[23] Our data for the flow with one vortex pairing show reasonable agreement with this scaling. This agreement could probably be improved considerably if the scaling law were not derived, based on the assumption that all particles affected by the mixing layer were redistributed evenly, but if instead the value of St would enter into this particle distribution function. However, this effect should be evaluated in a flow field that behaves more like a truly turbulent mixing layer.

For the case of horizontal flow, we can then distinguish three different settling and dispersion regimes: For relatively large terminal velocities, the particle settling is dominated by gravity, with a modulation due to the coherent vorticity, but without strong concentration nonuniformities. For intermediate settling velocities, the Kelvin–Helmholtz vortices are driving the ejection of particles into the opposite stream, along with the creation of depleted regions and regions of strong particle accumulation for moderate values of the Stokes number. These regions of large particle concentration take the forms of bands that persist in the lower free stream. Their asymptotic angle depends on the terminal settling velocity only, whereas their distance is also affected by the streamwise spacing between the vortices. Finally, for small terminal velocities there is a tendency of the mixing layer to suspend the particles. This tendency remains observable in the presence of vortex pairing, even though for such unsteady flows its importance diminishes.

For upward flow in which the faster stream is seeded (equivalent to downward flow with the slower stream being the seeded one), there exists a sharp optimum for the particle dispersion when the terminal settling velocity equals one-half the difference between the free-stream velocities. Under these conditions, the particles move at approximately the same streamwise velocity as the coherent vortices, so that the relatively small cross-stream fluid velocity components can affect the particles for sufficiently long times to entrain them into the mixing layer. Subsequently, the vortices eject them into the unseeded free stream. If the particles were seeded in the slower stream, cross-stream dispersion is very small.

A natural extension of the present work will try to account for the effect of the particles on the flow. Especially in regions of large particle accumulations and slip velocities, we have to expect significant momentum transfer from the particles to the fluid phase (Kiger and Lasheras[26]), which, in turn, will alter the fluid velocities. Furthermore, the coagulation and breakup of the particles and droplets may become important as well.

ACKNOWLEDGMENTS

Computing Resources were provided by the San Diego Supercomputer Center.

This work has been supported by the National Science Foundation under Grant No. CTS-9196004, and by the Electric Power Research Institute.

APPENDIX: ASYMPTOTIC ANALYSIS IN THE LIMIT Fr→0

In this appendix, we compare the $y(t)$ displacement of a particle settling in still fluid with that of a particle settling through the mixing layer. The latter particle can, in the process of settling, encounter a net upward or downward fluid motion, and it is of interest to establish if such a net fluid motion can result in a net change of the overall settling rate in the limit of Fr$\rightarrow$0. In this limit, only the y component of the equation of motion needs to be considered. Motivated by the velocity field of a mixing layer, and in the interest of mathematical simplicity, we approximate the upward fluid velocity component as $\exp(-2\pi/L|y|)$. The following analysis would proceed similarly for other approximations and lead to the same end result, although some of the mathematical details would be different. The resulting equation of motion is

$$\ddot{y}=\frac{1}{\mathrm{St}}\left[\exp\left(-\frac{2\pi}{L}|y|\right)-\dot{y}\right]-\frac{1}{\mathrm{Fr}^2}. \tag{A1}$$

Multiply Eq. (A1) by Fr^2 and let ϵ denote Fr^2, so that

$$\epsilon\ddot{y}+\frac{\epsilon}{\mathrm{St}}\dot{y}-\frac{\epsilon}{\mathrm{St}}\exp\left(-\frac{2\pi}{L}|y|\right)=-1, \tag{A2}$$

with the initial conditions, $y(0)=y_0$ and $\dot{y}(0)=v_0$. This is a highly singular problem and one can get a perturbation expansion in terms of ϵ. Before doing so, we solve the linear problem for the particle settling in still fluid,

$$y=y_0-\mathrm{St}\left(\frac{\mathrm{St}}{\mathrm{Fr}^2}+v_0\right)\left[\exp\left(-\frac{t}{\mathrm{St}}\right)-1\right]-\frac{\mathrm{St}}{\mathrm{Fr}^2}t. \tag{A3}$$

The exponential term in the above equation suggests the presence of a boundary layer solution. When the nonlinear mixing layer term is added, the above solution is modified. First, the inner expansion is done, for it can satisfy both of the initial conditions. Let $T=t/\mu(\epsilon)$, so that $\partial/\partial t=(1/\mu)(\partial/\partial T)$. The equation becomes

$$\frac{\epsilon}{\mu^2}\ddot{y}+\frac{\epsilon}{\mathrm{St}\mu}\dot{y}-\frac{\epsilon}{\mathrm{St}}\exp\left(-\frac{2\pi}{L}|y|\right)=-1, \tag{A4}$$

where the derivatives are with respect to T. On matching the first term and the fourth term we get $\mu=\sqrt{\epsilon}$. This distinguished limit yields the inner expansion. With this value of μ, the above equation becomes

$$\ddot{y}+\frac{\sqrt{\epsilon}}{\mathrm{St}}\dot{y}-\frac{\epsilon}{\mathrm{St}}\exp\left(-\frac{2\pi}{L}|y|\right)=-1, \tag{A5}$$

and the expansion series is

$$y=Y_0+\sqrt{\epsilon}Y_1+\epsilon Y_2+\cdots. \tag{A6}$$

The resulting solution is

$$y=y_0-\left(\frac{\mathrm{St}}{\epsilon}+v_0\right)\mathrm{St}\left[\exp\left(-\frac{\sqrt{\epsilon}T}{\mathrm{St}}\right)-1\right]-\frac{\mathrm{St}}{\epsilon}\sqrt{\epsilon}T+\frac{\epsilon}{\mathrm{St}}\int_0^T\int_0^T\exp\left(-\frac{2\pi}{L}\left|y_0+\sqrt{\epsilon}v_0T-\frac{T^2}{2}\right|\right)dT\,dT+O(\epsilon^{3/2}). \tag{A7}$$

The last term in the above equation gives the interaction effect due to the nonlinear fluid motion term, while the other terms correspond to the case of the particle settling in still fluid [Eq. (A3)]. The interaction term vanishes as $\mathrm{Fr}\to 0$. Since δ_d and δ_χ are proportional to y and $y^2/2$, respectively, their values approach those for settling in still fluid as $\mathrm{Fr}\to 0$.

[1] J. Martin and E. Meiburg, "The accumulation and dispersion of heavy particles in forced two-dimensional mixing layers. Part 1: The fundamental and subharmonic cases," Phys. Fluids A **6**, 1116 (1994).
[2] C. T. Crowe, R. A. Gore, and T. R. Troutt, "Particle dispersion by coherent structures in free shear flows," Part. Science Technol. **3**, 149 (1985).
[3] R. Chein and J. N. Chung, "Effects of vortex pairing on particle dispersion in turbulent shear flows," Int. J. Multiphase Flow **13**, 785 (1987).
[4] B. J. Lázaro and J. C. Lasheras, "Particle dispersion in a turbulent, plane, free shear layer," Phys. Fluids A **1**, 1035 (1989).
[5] B. J. Lázaro and J. C. Lasheras, "Particle dispersion in the developing free shear layer. Part 1. Unforced flow," J. Fluid Mech. **235**, 143 (1992).
[6] B. J. Lázaro and J. C. Lasheras, "Particle dispersion in the developing free shear layer. Part 2. Forced flow," J. Fluid Mech. **235**, 179 (1992).
[7] E. K. Longmire and J. K. Eaton, "Structure and control of particle-laden jet," J. Fluid Mech. **236**, 217 (1992).
[8] H. Stommel, "Trajectories of small bodies sinking slowly through convection cell," J. Marine Res. **8**, 24 (1949).
[9] M. R. Maxey and S. Corrsin, "Gravitational settling of aerosol particles in randomly oriented cellular flow fields," J. Atmos. Sci. **43**, 1112 (1986).
[10] M. R. Maxey, "Gravitational settling of aerosol particles in homogeneous and random flowfields," J. Fluid Mech., **174**, 441 (1987).
[11] L. P. Wang and M. R. Maxey, "Settling velocity and concentration distribution of heavy particles homogeneous isotropic turbulence," J. Fluid Mech. **256**, 27 (1993).
[12] M. J. Manton, "On the motion of a small particle in the atmosphere," Boundary Layer Meteorol. **6**, 487 (1974).
[13] A. M. Gañán-Calvo and J. C. Lasheras, "The dynamics and mixing of small spherical particles in a plane, free shear layer," Phys. Fluids A **3**, 1207 (1991).
[14] K.-K. Tio, A. M. Gañán-Calvo, and J. C. Lasheras, "The dynamics of small, heavy, rigid spherical particles in a periodic Stuart vortex flow," Phys. Fluids A **5**, 1679 (1993).
[15] J. B. Mclaughlin, "Particle size effects on Lagrangian turbulence," Phys. Fluids **31**, 2544 (1988).
[16] C. T. Crowe, J. N. Chung, and T. R. Troutt, "Particle dispersion by organized turbulent structures," *Particulate Two-Phase Flow*, edited by M. C. Roco (Butterworths, New York, 1993).
[17] J. K. Eaton and J. R. Fessler, "Preferential concentration of particles by turbulence," Int. J. Multiphase Flow **20**, 169 (1994).
[18] A. Michalke, "On the inviscid instability of the hyperbolic-tangent velocity profile," Phys. Fluids **19**, 543 (1964).
[19] M. R. Maxey and J. R. Riley, "Equation of motion for a small rigid sphere in a non-uniform flow," Phys. Fluids **26**, 883 (1983).
[20] L. P. Bernal and A. Roshko, "Streamwise vortex structures in plane mixing layers," J. Fluid Mech. **170**, 499 (1986).
[21] W. T. Ashurst and E. Meiburg, "Three-dimensional shear layers via vortex dynamics," J. Fluid Mech. **189**, 87 (1988).
[22] J. C. Lasheras and H. Choi, "Three-dimensional instability of a plane free shear layer. An experimental study of the formation and evolution of streamwise vortices," J. Fluid Mech. **189**, 53 (1988).
[23] F. K. Browand and B. O. Latigo, "Growth of the two-dimensional mixing layer from a turbulent and nonturbulent boundary layer," Phys. Fluids **22**, 1011 (1979).
[24] R. Clift, J. R. Grace, and M. E. Weber, *Bubbles, Drops and Particles* (Academic, New York, 1978).
[25] C. D. Winant and F. K. Browand, "Vortex pairing, the mechanism of turbulent mixing-layer growth at moderate Reynolds numbers," J. Fluid. Mech. **63**, 237 (1974).
[26] K. T. Kiger and J. C. Lasheras, "Effect of vortex pairing on particle dispersion and kinetic energy transfer in a two-phase turbulent shear layer," submitted to J. Fluid. Mech.
[27] E. Meiburg, P. K. Newton, N. Raju, and G. Ruetsch, "Unsteady models for the nonlinear evolution of the mixing layer," to appear Phys. Rev. E.